

Geodynamic Background of Intracontinental Cenozoic Alkaline Volcanic Rocks in Laojiezi, Western Yangtze Craton: Constraints from Sr-Nd-Hf-O Isotopes

YAN Qinggao^{1,2}, JIANG Xiaojun^{1,2,*}, LI Chao³, ZHOU Limin³, WANG Zhongqiang¹, Sultan Baig SHER^{1,4}, QU Wenjun³ and DU Andao³

1 Department of Earth Sciences, Faculty of Land Resource Engineering, Kunming University of Science and Technology, Kunming 650093, China

2 Beijing SHRIMP Center, Chinese Academy of Geological Sciences, Beijing 100037, China

3 National Research Center for Geoanalysis, Chinese Academy of Geological Sciences, Beijing 100037, China

4 Department of Earth Science, Karakoram International University, Gilgit-Baltistan, Pakistan

Abstract: The Laojiezi alkaline volcanic rocks, which are located in the intraplate region of the Yangtze craton, coincide with the formation of the Jinshajiang-Ailaoshan-Red River alkaline rock belt. Although this belt has been widely studied by geologists because of its porphyry-related Pb-Ag-Au polymetallic deposit and geotectonic location, the material sources of this belt are still debate. Whole-rock analyses show that these rocks have high total alkali contents (3.73–11.08wt%), and their aluminum saturation index (ASI) values widely vary from 0.82 to 3.07, which comprise a metaluminous-peraluminous magma series. These rocks are characterized by high K ($K_2O/Na_2O > 1$) and low Ti and Mg contents; enrichment in large-ion lithophile elements, such as Rb, Ba, K and light rare earth elements; and depletion in high field strength elements, such as Ta, Nb, P, and Ti. These rocks exhibit moderate Eu ($Eu/Eu^* = 0.86–1.04$) and Ce ($Ce/Ce^* = 0.63–0.96$) anomalies. Their ($^{87}Sr/^{86}Sr$), $\epsilon_{Nd}(t)$, zircon $\epsilon_{Hf}(t)$ and $\delta^{18}O$ values range from 0.70839 to 0.71013, from -10.16 to -12.45, from -19.6 to -5.8, and from 5.69‰ to 8.54‰, respectively, and their Nd and Hf two-stage model ages (T_{DM2}) are 1.67–1.86 Ga and 1.27–2.02 Ga, respectively. These data reflect the primary partial melting of Paleoproterozoic to Mesoproterozoic lower crust with minor residual continental lithospheric mantle and supracrustal metasediments. The lithosphere was likely thickened along the southeastern margin of the Tibetan Plateau following the Indian-Asian continent-continent collision (65–41 Ma). During the post-collision phase (36–16 Ma), the transition from a compressional to extensional setting triggered the convective removal of the over-thickened CLM beneath the Yangtze craton, which led to the upwelling of asthenospheric materials. This process created alkali-rich and high-K magma through the partial melting of the thickened lower crust. Magma that carried Cu-Au-Pb-Ag minerals was emplaced by strike-slip motion along the E- to W- or ENE- to WSW-trending tectonically weak zone, finally forming an alkaline porphyry Cu-Au-Pb-Ag polymetallic deposit.

Key words: Sr-Nd-Hf-O isotopes, alkaline volcanic rocks, post-collision, Laojiezi deposit, western Yangtze craton

1 Introduction

The Sanjiang region (Jinshajiang, Nujiang, and Lancangjiang) is located in the western Yangtze craton, SW China, along the southeastern margin of the Qinghai-Tibetan Plateau, which is a very active Cenozoic

continental deformation zone. This region represents a typical area for the study of Cenozoic lithospheric tectonic evolution and geodynamic processes around the world (Bi Xianwu et al., 2005). A large number of intraplate alkaline porphyry Cu-Au polymetallic deposits have been discovered in this belt in recent decades after the Jinshajiang-Red River alkaline intrusion belt was first

* Corresponding author. E-mail: cagsjiang@126.com

proposed by Professor Tu Guangchi (1984). Although many geologists have examined the mineralogy, petrology, geochemistry, magmatic stages and geochronology of this alkaline intrusion belt (e.g., Zhang Yuquan et al., 1997; Wang et al., 2001; Hu Ruizhong et al., 2004; Bi Xianwu et al., 2005; Lu et al., 2012, 2013a,b; Xu et al., 2012, 2014; Deng et al., 2014; Yang et al., 2016; Hou et al., 2007, 2017; Yang et al., 2017; Yan Qinggao et al., 2017; Wang et al., 2018; Xiao et al., 2018), the petrogenesis and magmatism of this belt still remain controversial. Multiple models have been proposed, including a continental subduction model, which is related to the eastward subduction of the Indian continent (Wang et al., 2001); a subduction and breakoff model that describes the breakoff of the Neo-Tethys oceanic crust, which was then subducted into the continental lithosphere of the Indian Block (Flower et al., 2013); a partial melting model of arc mantle, which represented melting that was triggered by Indian-China block extrusion and concomitant trans-lithospheric faulting (Hou et al., 2003; Wang Jianghua et al., 2003); a partial melting model that was related to metasomatic enriched mantle (Zhang Yuquan et al., 2000; Jiang Yaohui et al., 2006); a partial melting model of spinel harzburgite, which was metasomatized by fluids from the subducted Paleo-Tethys oceanic slab (Huang et al., 2006, 2007); and a delamination model of thickened lithospheric mantle (Deng et al., 2014, 2015; Lu et al., 2015).

The Laojiezi Cu-Au polymetallic deposit, Beiya gold-polymetallic deposits and Machangqing Cu-Mo (Au) polymetallic deposits are located in the middle and southern regions of the Cenozoic Jinshajiang-Ailaoshan alkaline intrusion belt in the western Yangtze craton and in the western Yunnan region. These deposits formed at a similar time under the same tectonic setting (Fig. 1). The Beiya intrusions were derived from the partial melting of a crust-mantle transitional zone and continental lithospheric mantle (CLM), where they were influenced by the subduction of oceanic plates. Their diagenetic age ranges from 32.5 Ma to 36.9 Ma, and their metallogenic age is 36.87 ± 0.76 Ma (Lu et al., 2012; He Wenyan et al., 2013). The Machangqing intrusion complex was derived from the partial melting of thickened lower crust or the mixture of crust-derived and mantle-derived magma; its diagenetic age is approximately 35 Ma and its metallogenic age ranges from 33.9 Ma to 35.8 Ma (Wang Denghong et al., 2004; Zeng Pusheng et al., 2006; Liang Huaying et al., 2004, 2007; Lu et al., 2013a). The Laojiezi alkaline intrusion is located in the intraplate region of the Yangtze craton, far from the Jinshajiang-Ailaoshan suture (>150 km), which is also consistent with the formation of the Jinshajiang-Ailaoshan alkaline volcano-magmatic

complex belt. However, its material source, petrogenesis, and geodynamic setting also remain controversial. Bi Xianwu et al. (2005) and Chen Jin et al. (2007) proposed that the Laojiezi alkaline complex originated from enriched mantle (EM II), which is characterized by crust-mantle mixing. Li Yong et al. (2011) believed that this complex was derived from the partial melting of the mantle, which was induced by the Indian-Asian continent-continent collision when the tectonic regime was changing. Rui Zhongyao and Hou Zengqian (2006) proposed that the ultra-shallow intrusion of the alkaline porphyry belt originated from the mixture of crust-derived and mantle-derived magma but mainly from mantle-derived magma. Lu et al. (2013a) believed that this complex was derived from the fractional crystallization of lamprophyres from the metasomatized lithospheric mantle.

We obtain whole-rock geochemistry data from the Laojiezi alkaline volcanic rocks and performed Sr-Nd and in-situ zircon Hf-O isotope analyses to constrain their material source, petrogenesis, and geodynamic setting. The new findings in this paper should improve our understanding of the Cenozoic deep stratigraphic structure and shallow crustal geologic processes and provide important information for the implementation of external and deep mineral prediction in the Laojiezi Pb-Ag polymetallic deposit. These data indicate that mineralization occurred both along the margin of the plate and in the intraplate region.

2 Geological Settings

The Laojiezi alkaline volcanic rocks are exposed in the Cultural village-Laojiezi village-Baimaju village area, Yao'an County, central Yunnan Province. This region is located within the Chuxiong Mesozoic basin in the western intraplate region of the Yangtze craton, located far from the Jinshajiang-Ailaoshan suture (>150 km) along the southeastern margin of the Qinghai-Tibetan Plateau (Fig. 2). These rocks are an important component of the Jinshajiang-Ailaoshan-Red River alkaline porphyry zone. Mainly Mesozoic and Cenozoic strata are exposed, most of which are red layers from the Cenozoic era; only a few Pliocene strata and Oligocene volcanic-clastic strata are exposed in the vicinity of the Laojiezi Pb-Ag polymetallic deposit. The lower Cretaceous Gaofengsi formation (K_{1w}) and Puchanghe formation (K_{1p}) and the upper Cretaceous Matoushan formation (K_{2m}) and Jiangdihe formation (K_{2j}) are the main Mesozoic strata. The Oligocene Laojiezi formation (E_3l) and Pliocene strata (N_2) are the main Cenozoic strata in the study area. The top of the Cenozoic strata are trachyte volcanic-clastic strata from the Oligocene Laojiezi formation (E_3l), which has been

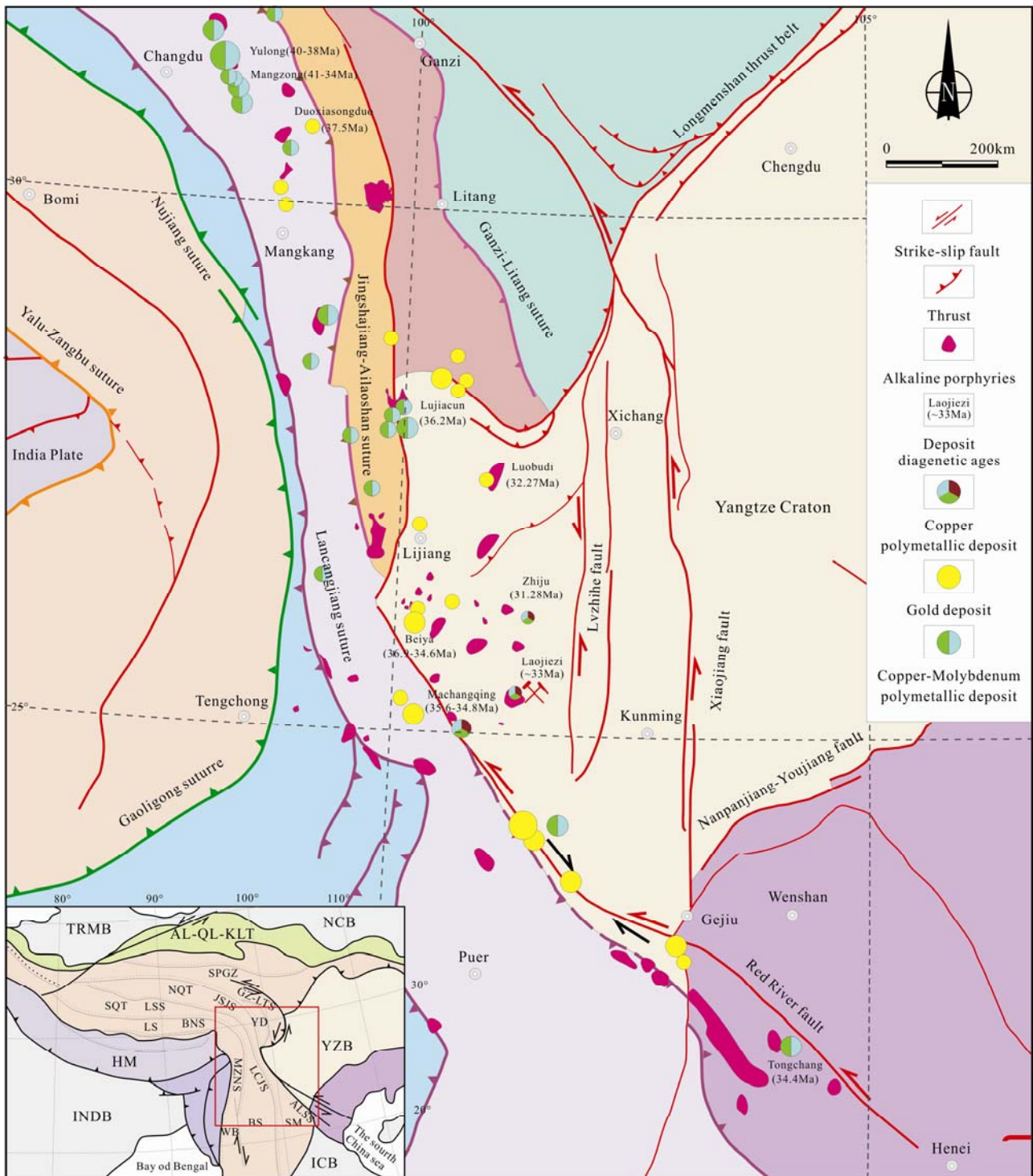


Fig. 1. Geologic map showing the distribution of Cenozoic alkaline porphyry and its tectonic of the southeastern margin of the Qinghai-Tibet Plateau (modified from Hou Zengqian et al., 2006; Li Wenchang et al., 2009; Ren Jishun et al., 2013).

divided into a complete volcanic edifice that contains, from the center to the edge, a volcanic facies, eruptive facies, eruptive overflowing facies, and eruptive sedimentary facies. These facies were replaced by syenite porphyry, which is the main lead and silver ore-bearing strata in this deposit. The strata mainly comprise syenite agglomerate, pseudoleucite trachyte, trachytic volcanic

agglomerate, trachytic tuff, trachytic tuff with breccia and tuffaceous clastic rock, among others, which are mainly distributed in the Laojiezi deposit, Laojiezi village, Liujia village, Caiyuan village and Dalongtan reservoir. These rocks can be compared to the volcanic rocks from the Jianchuan formation, which are spread throughout Jianchuan County, Wa'se County, Binchuan County and

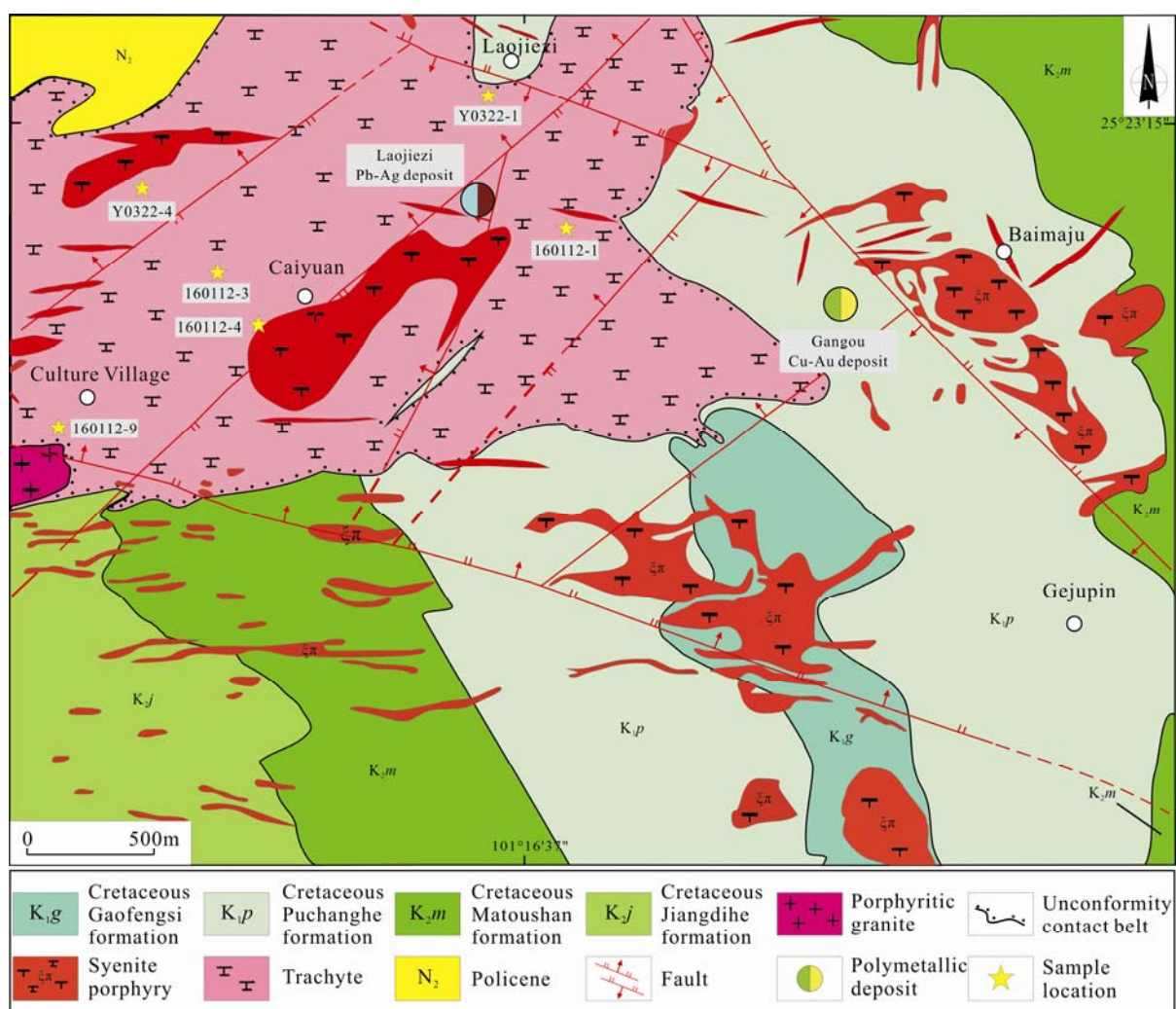


Fig. 2. Simplified geologic map showing the distribution of the Laojiezi alkaline volcanic-magmatic complex.

Midu County in this region. The alkaline volcanic rocks from the Laojiezi formation contain a complete volcanic edifice, including a volcanic conduit facies (syenite agglomerate), eruptive facies (trachytic volcanic agglomerate), eruptive overflowing facies (ignimbrite and pseudoleucite trachyte), eruptive sedimentary facies (tuff), and fluvial and lake facies (tuffaceous conglomerate and sandstone). The alkaline volcanic rocks formed from 33.67 Ma to 33.27 Ma based on the zircon SHRIMP U-Pb ages of trachytic tuff with breccia (Y0322-1) and trachytic ignimbrite (Y0322-4) (Yan Qinggao et al., 2017). The alkaline volcanic-magmatic complex comprises syenite porphyry, porphyritic granite, syenite-aplite and other intrusions, which were emplaced as veins, stocks and few dikes. Most of the contact lines between the intrusions and country rocks are regular and clear, with many obvious joints reflecting the injections of later quartz and/or calcite fluid in the vicinity of the contact zone. Hornfels formed in the contact segments of partial country rocks because of hydrothermal or thermal metamorphism. The phenomenon

of fading between intrusions and country rocks is obvious, which is mainly reflected by color transitions and the compositional alteration of material. The Laojiezi Pb-Ag polymetallic ore bodies and Gangou Cu-Au polymetallic ore bodies were mainly deposited in Mesozoic red layers, Oligocene trachytic tuff and porphyritic granite, and other tectonic spaces where fissures and interstitial zones were well developed and controlled by NE- and NW-trending tectonic zones (Fig. 2).

3 Samples and Petrography

Six samples of alkaline volcanic rocks from the Laojiezi formation (E_2l) were collected from the vicinity of Laojiezi village (Figs. 2–3), which were used to analyze their whole-rock Sr-Nd isotopes and major and trace elements. The trachytic tuff with breccia (Y0322-1) and trachytic ignimbrite (Y0322-4) underwent zircon SHRIMP O isotopic and LA-MC-ICP-MS Hf isotopic analyses. Brief descriptions of these samples are summarized in

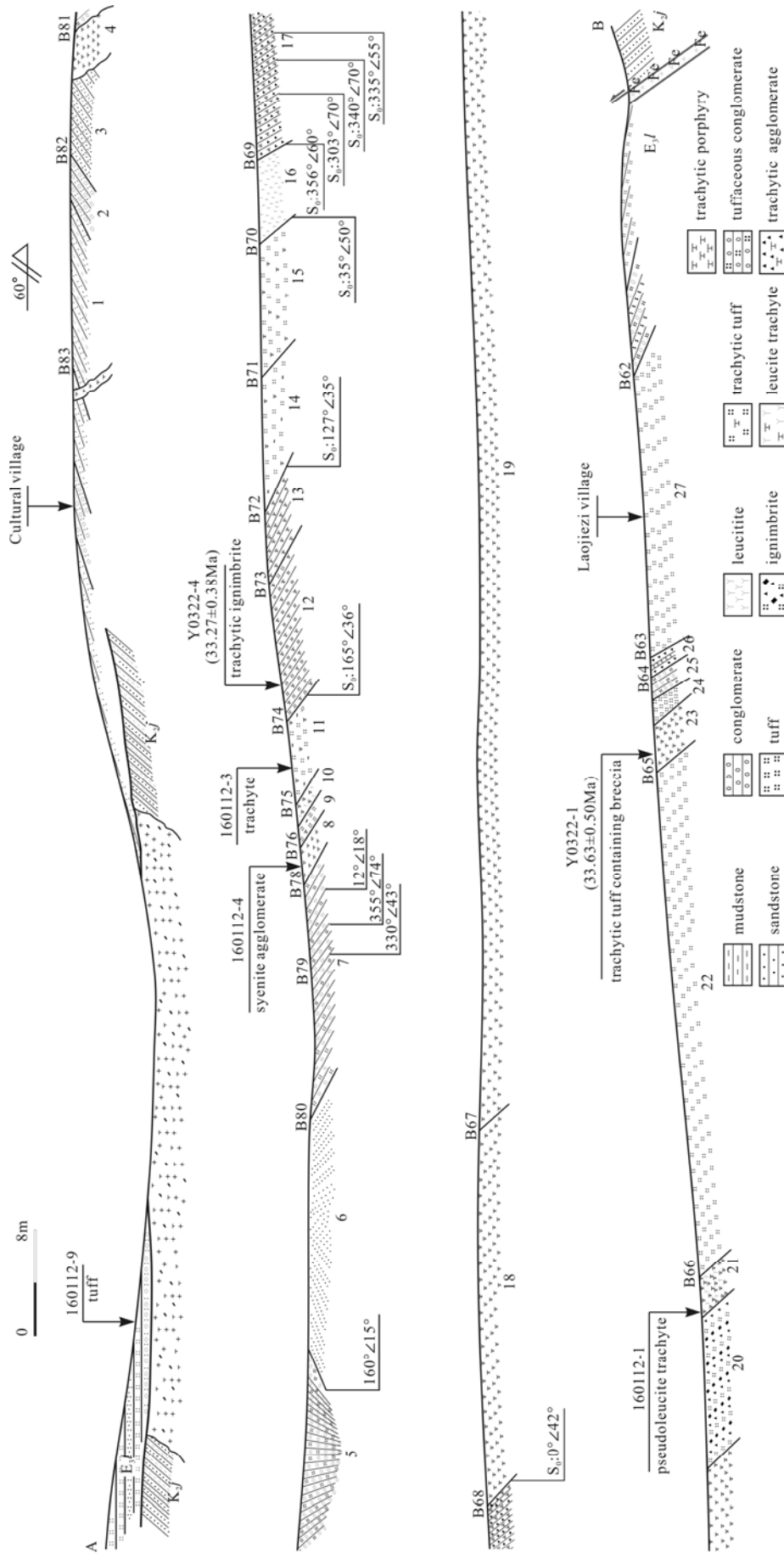


Fig. 3. Measured section of the Laojiezi alkaline volcano-magmatic complex and its samples location.

Table 1.

The trachytic ignimbrite (Y0322-4) belongs to the effusion subfacies; this sample grayish, grayish-white and grayish-green, with porphyritic texture and a compact block structure. This rock mainly consists of garnet with

alternating feldspar and biotite, and grayish-white phenocrysts of flat garnet can be observed in the field (Fig. 4a). Under the microscope, the minerals are mainly garnet with alternating quartz and potassic feldspar, alongside minor biotite and amphibole. The phenocrysts

Table 1 Brief description of Laojiezi alkaline volcanic rocks, western Yangtze craton

| Sample | Locality | Rock type | SiO ₂ (wt%) | Mg [#] | Phenocrysts | Groundmass | Accessory | Alteration |
|----------|----------|----------------------------------|------------------------|-----------------|----------------|----------------|-----------|-------------------------------|
| Y0322-4 | Yao'an | Trachytic ignimbrite | 56.55 | 0.23 | Kfs+Lct+Qtz+Bt | Kfs+Lct+Qtz+Bt | Ap+Sp+Zr | Strong Kfs+Srt alteration |
| 160112-1 | Yao'an | Pseudoleucite trachyte | 55.05 | 0.08 | Lct | Or+Kfs | Ne+Mt | Strong Kfs+Srt+Kal alteration |
| Y0322-1 | Yao'an | Trachytic tuff contained breccia | 55.78 | 0.20 | Kfs+Qtz | Kfs+Qtz+Or | Hb+Ap | Moderate alteration |
| 160112-3 | Yao'an | Trachyte | 61.63 | 0.24 | Qtz+Plag+Bt | Qtz+Plag+Bt | Hb+Cpx | Moderate alteration |
| 160112-4 | Yao'an | Syenite agglomerate | 68.06 | 0.12 | Or+Plag+Bt | Or+Plag+Bt | Hb | Unaltered |
| 160112-9 | Yao'an | Tuff | 65.12 | 0.28 | — | Or+Qtz+Bt | Hb | Moderate alteration |

Abbreviations: Ap=apatite, Bt=biotite, Cpx=clinopyroxene, Hb=hornblende, Kfs=K-feldspar, Lct=leucite, Ne=nephelite, Or=orthoclase, Plag=plagioclase, Qtz=quartz, Srt=sericite, Zr=zircon Mt=magnetite; Mg[#]=MgO/(MgO+Fe₂O₃ (total)) in atomic ratio (from Table 2).

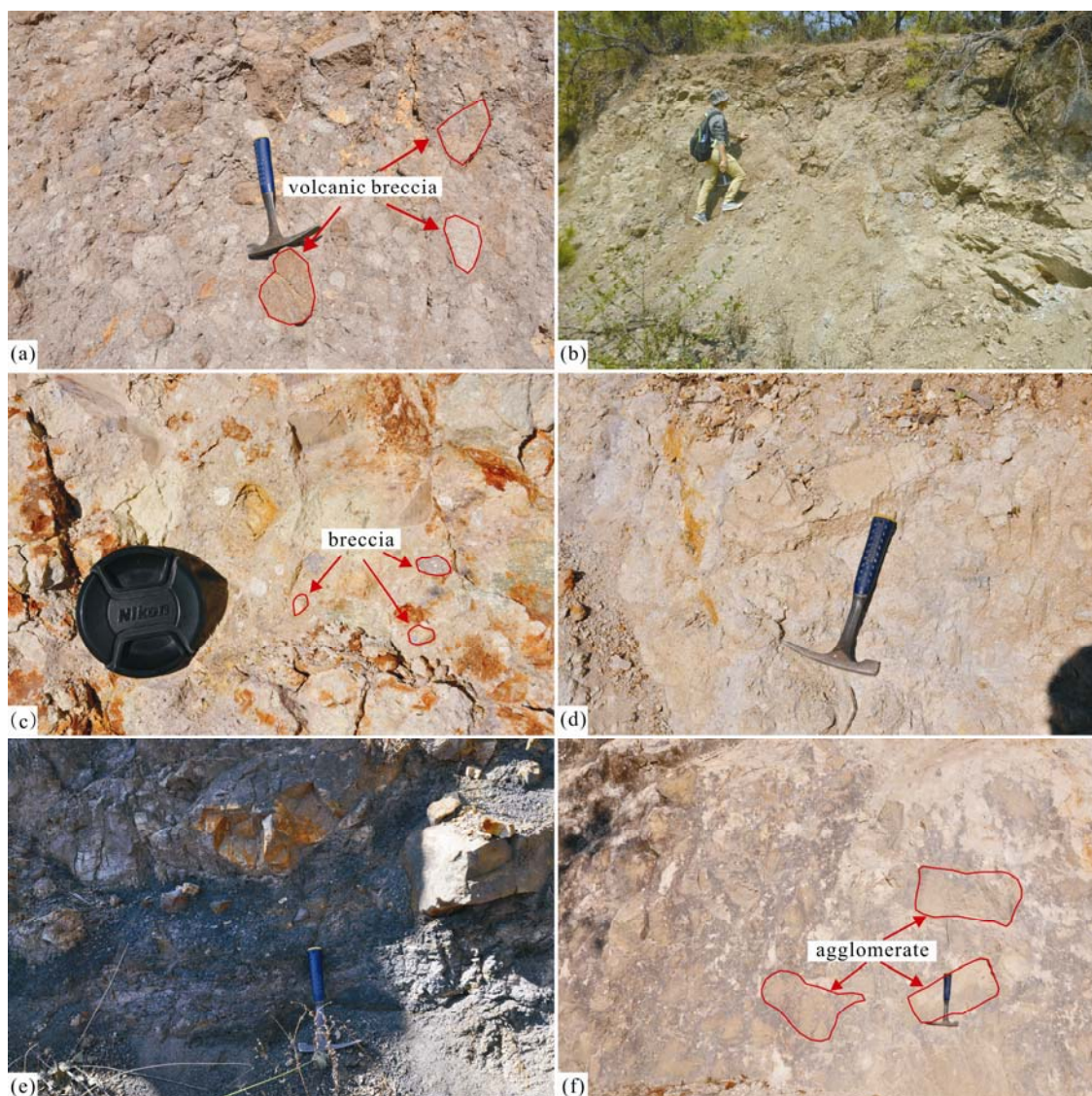


Fig. 4. Photographs showing the characteristics of field petrography for Laojiezi alkaline volcanic rocks, western Yangtze craton.

(a), Trachytic ignimbrite, has a comparatively medium size (about 5–20cm) of volcanic breccias. Photograph from the same locality as sample Y0322-4; (b), pseudoleucite trachyte, photograph from the same locality as sample 160112-1; (c), trachytic tuff contained breccias, has a comparatively smaller size (about 0.5–5cm) of breccias. Photograph from the same locality as sample Y0322-1; (d), trachyte, photograph from the same locality as sample 160112-3; (e), tuff, Photograph from the same locality as sample 160112-9; (f), syenite agglomerate, has a comparatively large size (about 25–60cm) of agglomerate, the agglomerate composed by syenite porphyry. Photograph from the same locality as sample 160112-4.

are mainly pseudoleucite, which exhibit tetragonal trioctahedra or bands, and the pseudoleucite alterations are mainly potassic feldspathization, kaolinization, and sericitization. The quartz phenocrysts have dissolved into harbor-like shapes. The substrate is cryptocrystalline; its composition is similar to that of the phenocrysts, and this sample is accompanied by a vesicular structure with tiny strips of microcrystalline feldspars that are intertwined or weakly aligned. The accessory minerals are mainly apatite, sphene, and minor zircon (Fig. 5a).

The pseudoleucite trachyte (160112-1) belongs to the

effusion subfacies; this sample grayish-green and grayish-white, although some portions are canary, with porphyritic textures and block structures. The pseudoleucite phenocrysts have undergone kaolinization alteration, which formed grayish-white or tan, octagonal or round grains (Fig. 4b). Under the microscope, the pseudoleucite phenocrysts are octagonal or round, with particle sizes of 2–3 mm. The pseudoleucite has strong alkali feldspar (K-feldspar) alteration, showing clear residual metasomatism; some of the pseudoleucite alteration is sericitization and kaolinization. The substrate is a micromatrix that consists

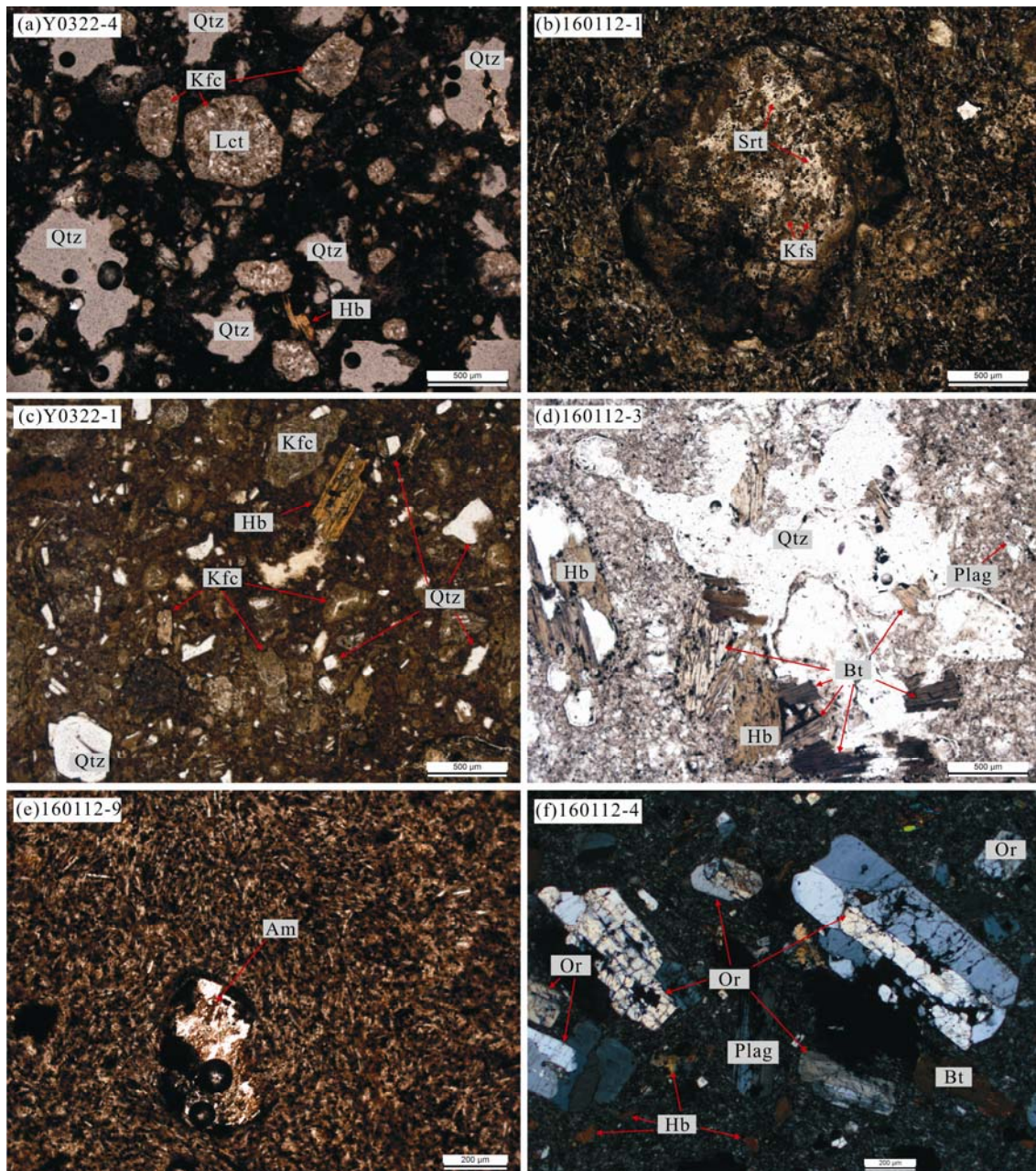


Fig. 5. Photomicrographs of Laojiezi alkaline volcanic rocks, western Yangtze craton.

(a), Trachytic ignimbrite (Y0322-4); (b), pseudoleucite trachyte (160112-1); (c), trachytic tuff contained breccias (Y0322-1); (d), trachyte (160112-3); (e), tuff (160112-9); (f), syenite agglomerate (160112-4). Abbreviations: Bt=biotite, Hb=hornblende, Srt=sericite, Kfs=K-feldspar, Lct=leucite, Plag=plagioclase, Qtz=quartz, Am=amphibole xenolith.

of tiny strips of weakly aligned microcrystalline feldspar (with particle sizes less than 0.2 mm). The accessory minerals are mainly nephelinite and minor magnetite (Fig. 5b).

The trachytic tuff with breccia (Y0322-1) belongs to the volcanic-sedimentary facies; this sample is grayish-white and grayish-brown, with tuff textures and block-brecciated structures. This rock mainly consists of volcanic ash, volcanic debris, and volcanic breccia. The breccia particle sizes are 0.5–5 cm (Fig. 4c). Under the microscope, the minerals are mainly K-feldspar, quartz, and minor biotite; the K-feldspar grains exhibit idiomorphic or hypidiomorphic granular structures, with particle sizes of <0.5 mm. The quartz grains show harbor-like shapes or are granular, and the biotite is sliced and fractured. The substrate is cryptocrystalline and consists of aligned feldspar and volcanic glass. The accessory minerals are mainly hornblende and apatite (Fig. 5c).

The trachyte (160112-3) belongs to the explosive facies; this sample is light gray, with tuff textures and block structures, and mainly comprises alkali feldspar, plagioclase and a few dark minerals (Fig. 4d). The dark minerals mainly consist of biotite, minor hornblende, and clinopyroxene. Hypidiomorphic quartz exhibits corrosion with biotite and hornblende, which aggregate to form intertwined phenocrysts. The composition of the substrate is similar to that of the phenocrysts, and the sample has a holocrystalline trachytic texture. The accessory minerals are mainly hornblende and alkali pyroxene (Fig. 5d).

The tuff (160112-9) belongs to the volcanic-sedimentary facies; this sample is grayish-white, but its weathering surface is grayish-green, with tuff textures and block structures. This rock mainly consists of tephra, which comprises feldspar, quartz and a few dark minerals (Fig. 4e). The substrate is cryptocrystalline, with an intertexture structure accompanied by a vesicular structure, and the sample mainly consists of granule-banded feldspar, minor biotite and hornblende and fragments of volcanic glass. Furthermore, this rock contains amphibole xenoliths (Fig. 5e), which may represent direct samples of Neoproterozoic fertilized cratonic lower continental crust (Hou et al., 2017).

The syenite agglomerate (160112-4) belongs to the subvolcanic facies; this sample is grayish-white and exhibits a porphyritic texture and block structure. Syenite agglomerate (with particle sizes of 25–60 cm) is embedded in the surrounding rock; the agglomerate is syenite porphyry, which is consistent with the characteristics of the surrounding rock (Fig. 4f). Under the microscope, the orthoclase phenocrysts are characterized by idiomorphic or hypidiomorphic textures, wide plate structures, particle sizes of 2–3 mm, and abundant

fractures. The plagioclase phenocrysts are lath-shaped, with albite twins. The composition of the substrate is similar to that of the phenocrysts; this rock has a cryptocrystalline texture that mainly consists of feldspar microcrystalline, biotite, and hornblende. The accessory minerals are mainly hornblende (Fig. 5f).

4 Analytical Methods

Whole-rock major- and trace-element and Sr-Nd and zircon Hf isotopic analyses were conducted at the National Research Center for Geoanalysis in Beijing. Zircon O isotopic analysis was undertaken on a SHRIMP II e-MC instrument at the Beijing SHRIMP Center (National Science and Technology Infrastructure), Beijing.

4.1 Major- and trace-element analyses

The samples that were used for the major- and trace-element analyses were crushed and ground into 200-mesh powders in a swing mill. Major elements were analyzed by using an inductively coupled plasma emission spectrometer (ICP-AES) with relative analytical uncertainties of >5%. Trace elements and rare earth elements (REE) were analyzed by using an inductively coupled plasma mass spectrometer (ICP-MS). The analytical uncertainties were less than 5%, and the reference material was GSR1. The detailed analytical procedures were described by Liu Yongsheng et al. (2013).

4.2 Zircon oxygen isotopic analyses

Zircon O isotopes were analyzed by using a sensitive high-resolution ion microprobe emission mass spectrometer (SHRIMP II e-MC); the detailed analytical procedures were described by Zhou Liqin et al. (2012). Prior to the zircon oxygen isotopic analyses, U-Pb isotopic analyses were performed by using the sensitive high-resolution ion microprobe (SHRIMP II) at the Beijing SHRIMP Center. Detailed U-Pb age data were previously published by Yan Qingao et al. (2017). The SHRIMP zircon ages are cited in Fig. 9. On each zircon, the oxygen analysis spot was placed close to the SHRIMP pit within a domain of uniform CL texture. The Gaussian $^{133}\text{Cs}^+$ primary ion beam was accelerated to 15kV, with an intensity of 3nA. A Kimball Physics ELG-5 electron flood gun was used to compensate for sample charging during analysis, with approximately 350eV of electrons. Negative secondary ions were extracted with a -10keV potential. $^{16}\text{O}^-$ and $^{18}\text{O}^-$ were measured in a Keithley 642 electrometer with a Faraday cup. The analysis time was approximately 2.5 min; each point was analyzed twice, consisting of 10s of pre-sputtering, automatic secondary

beam centering and 6×10 s intervals of oxygen isotope intensities. The $^{18}\text{O}/^{16}\text{O}$ ratios were reported in delta notation as $\delta^{18}\text{O}$ values by normalizing to a V-SMOW ($^{18}\text{O}/^{16}\text{O}$) value of $v_{\text{SMOW}}=0.0020052$ (Baertschi, 1976) and using an instrument mass fractionation factor (IMF), that is: $\delta^{18}\text{O}_{\text{Sample}}=(\delta^{18}\text{O})_{\text{M}}+\text{IMF}$, $(\delta^{18}\text{O})_{\text{M}}=((^{18}\text{O}/^{16}\text{O})_{\text{M}}/0.0020052-1) \times 1000(\text{‰})$, $\text{IMF}=(\delta^{18}\text{O})_{\text{M}}(\text{standard})-(\delta^{18}\text{O})_{\text{VSMOW}}$. The internal standard that was used for the mass-fractionation correction was the zircon 91500, which has a $\delta^{18}\text{O}$ value of 9.9‰ (Wiedenbeck et al., 2010).

4.3 Zircon hafnium isotopes

Hf isotope analyses were conducted by using a laser-ablation multi-collector inductively coupled plasma mass spectrometer (LA-MC-ICP-MS); the detailed analytical procedures were described by Hou Kejun et al. (2007). The Hf analyses were performed on the same spots as the previous oxygen isotope analyses, with a beam diameter of 40–60 μm , and helium carrier gas transported the ablated aliquot from the laser-ablation cell via a mixing chamber to the ICP-MS torch. The zircon standard GJ1 was analyzed to evaluate the accuracy of the laser-ablation results. Throughout the session, GJ1 yielded a mean value of $^{176}\text{Hf}/^{177}\text{Hf}=0.282015 \pm 8$ (2σ , $n=10$), which was consistent with the recommended value (within error) that was proposed by Elhlou et al. (2006). To calculate the ε_{Hf} values, we adopted the chondritic values of Bichert-Toft et al. (1997), that is, $(^{176}\text{Hf}/^{177}\text{Hf})_{\text{CHUR}}=0.032$ and $(^{176}\text{Hf}/^{177}\text{Hf})_{\text{CHUR0}}=0.282772$. We also used the decay constant $\lambda=1.865 \times 10^{-11} \text{ year}^{-1}$ (Scherer et al., 2006) in the ε_{Hf} calculations. To calculate depleted-mantle model ages (T_{DM1}), we adopted the values of $(^{176}\text{Lu}/^{177}\text{Hf})_{\text{DM}}=0.0384$ and $(^{176}\text{Hf}/^{177}\text{Hf})_{\text{DM}}=0.28325$ (Griffin et al., 2000). Here, we calculated two-stage model ages (T_{DM2}), which assumed that the parental magma was produced from average continental crust (i.e., $^{176}\text{Lu}/^{177}\text{Hf}=0.015$) that was derived from depleted mantle (Griffin et al., 2002).

4.4 Sr-Nd isotopic analyses

Following the separation of Rb, Sr, Sm and Nd in mineral and whole-rock samples by using selective specific resins, we obtained solutions that were rich in Sr and Nd. We analyzed the Sr and Nd isotopes by using a multicollector inductively coupled plasma mass spectrometer (MC-ICP-MS, NEPTUNE Plus). Throughout the analytical period, the Sr and Nd blanks were 10^{-9} – 10^{-10} g Sr and 5×10^{-11} g Nd, respectively, and the $^{87}\text{Rb}/^{86}\text{Sr}$ and $^{147}\text{Sm}/^{144}\text{Nd}$ ratios were calculated by using the whole-rock Rb, Sr, Sm and Nd concentrations from MC-ICP-MS (Table 2). The analyzed Sr and Nd isotopic ratios were corrected by normalizing to values of $^{88}\text{Sr}/^{86}\text{Sr}=8.37521$ and $^{146}\text{Nd}/^{144}\text{Nd}=0.7219$, respectively.

The measured Sr standard of SRM987 (America, National Institute of Standards and Technology, NIST) yielded a value of $^{87}\text{Sr}/^{86}\text{Sr}=0.710427 \pm 0.000012$ (2σ , $n=5$), while the Nd standard of JMC321 yielded a value of $^{143}\text{Nd}/^{144}\text{Nd}=0.511124 \pm 0.000010$ (2σ , $n=8$). The detailed analytical procedures were described by Tang Suohan et al. (2010) and He Xuexian et al. (2007).

5 Results

5.1 Major and trace elements

The major- and trace-element data are listed in Table 2. The rocks showed high SiO_2 contents of 55.05–68.06wt%, with $\text{K}_2\text{O}+\text{Na}_2\text{O}$ contents of 3.73–11.08wt%, $\text{K}_2\text{O}/\text{Na}_2\text{O}$ values of 1.33 to 30.48 and aluminum index (ASI) values that were characterized by A/CNK ratios of 0.82–3.07 and A/NK ratios of 1.13–4.05. These rocks had moderate Al_2O_3 (14.89–18.85wt%), K_2O (3.15–10.73wt%), and MgO (2.35–7.85wt%) contents and low Na_2O (0.13–4.13wt%), $^{\text{T}}\text{Fe}_2\text{O}_3$ (total Fe, 0.32–2.24wt%), and TiO_2 (0.30–1.25wt%) contents. On the A/CNK-A/NK classification diagram, the rocks fell within the metaluminous and peraluminous fields. These characteristics suggest that all the samples belonged to alkali-rich, high-K and metaluminous-peraluminous series, which are associated with basaltic trachyandesite, trachyandesite, tephriphonolite, and trachyte-trachydacite (Figs. 6a–c).

The alkaline volcanic rocks had light rare earth element (LREE) contents of 372.7–1120.8 ppm, with an average value of 816.7 ppm, and lower heavy rare earth element (HREE) contents of 34.4–158.7 ppm, with an average value of 89.1 ppm. All the analyzed samples were characterized by strong light rare earth element (LREE) enrichment, with $(\text{La}/\text{Yb})_{\text{N}}$ ratios of 37.87–67.32, $(\text{La}/\text{Sm})_{\text{N}}$ ratios of 4.04–8.07 and $(\text{Gd}/\text{Yb})_{\text{N}}$ ratios of 3.10–5.78. Their LREE/HREE ratios ranged from 7.1 to 12.7 and exhibited strong deviations. These rocks had slightly negative Eu and Ce anomalies, with Eu/Eu^* values of 0.86–1.04 and Ce/Ce^* values of 0.63–0.96. All the above characteristics were similar to those of continental tholeiite (Fig. 7a). The primitive mantle-normalized diagram (Fig. 7b) suggested that all the samples were enriched in large-ion lithophile elements (LILE; Rb, Ba, K, and LREEs), depleted in high-field-strength elements (HFSE, Ta, Nb, Hf, and HREEs), and strongly depleted in P and Ti (Fig. 7b).

5.2 Whole-rock Sr-Nd isotopes

The results of the Sr-Nd isotopic analyses are listed in Table 3 and illustrated in Fig. 8. All these rocks showed similar Sr and Nd isotopic compositions. The six samples had $^{87}\text{Rb}/^{86}\text{Sr}$ ratios from 0.14514 to 1.06470, with an

Table 2 The analytical results of major oxides (wt%), trace and rare elements (ppm) of the Laojiezi alkaline volcanic rocks, western Yangtze craton

| Sample | Y0322-4 | 160112-1 | Y0322-1 | 160112-3 | 160112-4 | 160112-9 |
|---|----------------------|------------------------|----------------------------------|----------|---------------------|----------|
| | Trachytic ignimbrite | Pseudoleucite trachyte | Trachytic tuff contained breccia | Trachyte | Syenite agglonerate | Tuff |
| Major oxides (wt%) | | | | | | |
| Na ₂ O | 3.70 | 0.35 | 0.58 | 3.30 | 3.65 | 4.13 |
| MgO | 2.24 | 0.72 | 1.51 | 1.27 | 0.32 | 1.37 |
| Al ₂ O ₃ | 14.89 | 18.85 | 17.68 | 17.54 | 16.49 | 15.77 |
| SiO ₂ | 56.55 | 55.05 | 55.78 | 61.63 | 68.06 | 65.12 |
| P ₂ O ₅ | 1.37 | 0.08 | 1.01 | 0.16 | 0.05 | 0.33 |
| K ₂ O | 6.60 | 10.73 | 3.15 | 7.03 | 5.37 | 5.50 |
| CaO | 2.68 | 0.19 | 0.76 | 0.60 | 0.54 | 1.81 |
| TiO ₂ | 0.97 | 0.99 | 1.25 | 0.65 | 0.30 | 0.43 |
| MnO | 0.10 | 0.03 | 0.01 | 0.02 | 0.00 | 0.03 |
| trace | 1.79 | 2.01 | 1.98 | 1.13 | 0.59 | 0.60 |
| LOI | 0.97 | 2.77 | 8.15 | 2.11 | 2.27 | 1.02 |
| ^T Fe ₂ O ₃ | 7.52 | 7.85 | 5.88 | 4.05 | 2.35 | 3.53 |
| Total | 99.39 | 99.61 | 97.74 | 99.49 | 99.98 | 99.64 |
| K ₂ O+Na ₂ O | 10.30 | 11.08 | 3.73 | 10.33 | 9.02 | 9.63 |
| K ₂ O/Na ₂ O | 1.79 | 30.48 | 5.48 | 2.13 | 1.47 | 1.33 |
| Trace elements (ppm) | | | | | | |
| Li | 22.5 | 23.9 | 9.3 | 13.0 | 8.3 | 15.0 |
| Be | 10.7 | 7.5 | 11.2 | 5.3 | 5.8 | 3.5 |
| Sc | 12.5 | 4.9 | 14.5 | 5.2 | 3.0 | 9.9 |
| Ti | 6661 | 5821 | 7754 | 4120 | 1576 | 6076 |
| V | 220.5 | 186.5 | 118.5 | 77.1 | 29.6 | 130.0 |
| Cr | 127.0 | 133.6 | 232.4 | 122.6 | 30.3 | 23.2 |
| Mn | 822.9 | 189.4 | 79.5 | 120.0 | 21.0 | 331.7 |
| Co | 17.8 | 9.9 | 14.3 | 7.3 | 3.0 | 4.9 |
| Ni | 116.0 | 117.6 | 158.5 | 69.3 | 22.3 | 35.6 |
| Cu | 24.9 | 32.4 | 32.0 | 11.5 | 3.3 | 12.4 |
| Zn | 293.5 | 125.0 | 1397.9 | 207.8 | 260.1 | 249.8 |
| Ga | 23.8 | 25.0 | 24.3 | 23.2 | 21.0 | 22.7 |
| Ge | 1.5 | 1.3 | 1.3 | 1.1 | 1.1 | 1.5 |
| As | 6.7 | 12.1 | 5.9 | 6.4 | 5.6 | 8.7 |
| Rb | 233.8 | 411.6 | 146.6 | 194.8 | 203.9 | 184.9 |
| Sr | 3819 | 1463 | 3821 | 2727 | 1151 | 3908 |
| Zr | 904.8 | 1505.2 | 943.7 | 621.7 | 418.7 | 773.1 |
| Nb | 33.8 | 46.5 | 33.5 | 24.2 | 29.7 | 32.2 |
| Mo | 5.3 | 12.9 | 14.5 | 8.4 | 4.9 | 1.6 |
| Ag | 7.12 | 13.66 | 8.376 | 5.415 | 4.481 | 9.426 |
| Cd | 0.1 | 0.1 | 0.5 | 0.2 | 0.2 | 0.1 |
| In | 0.1 | 0.1 | 0.1 | 0.0 | 0.0 | 0.1 |
| Sn | 3.8 | 5.2 | 4.7 | 2.9 | 2.6 | 2.8 |
| Sb | 0.3 | 0.9 | 0.6 | 0.9 | 1.0 | 0.1 |
| Cs | 1.5 | 1.4 | 5.2 | 4.9 | 4.6 | 3.3 |
| Ba | 9538 | 10405 | 8559 | 4685 | 2136 | 10139 |
| Hf | 19.4 | 29.1 | 19.4 | 12.3 | 9.5 | 15.9 |
| Ta | 1.6 | 2.1 | 1.7 | 1.3 | 1.8 | 1.7 |
| W | 5.9 | 8.1 | 3.1 | 7.8 | 4.4 | 6.4 |
| Hg | 0.7 | 0.8 | 0.4 | 0.9 | 0.4 | 0.8 |
| Tl | 1.7 | 2.3 | 1.5 | 2.1 | 1.2 | 0.6 |
| Pb | 374.7 | 103.5 | 344.1 | 137.6 | 92.7 | 69.1 |
| Bi | 0.1 | 0.2 | 0.2 | 0.3 | 0.1 | 0.0 |
| Th | 44.5 | 57.5 | 39.4 | 44.8 | 46.0 | 30.8 |
| U | 5.9 | 8.4 | 7.4 | 8.3 | 8.3 | 9.8 |
| Rare elements(ppm) | | | | | | |
| La | 281.8 | 280.6 | 284.9 | 187.1 | 118.9 | 181.8 |
| Ce | 527.8 | 338.0 | 503.3 | 326.6 | 161.6 | 304.7 |
| Pr | 54.8 | 51.4 | 63.2 | 33.5 | 19.9 | 35.7 |
| Nd | 216.5 | 164.2 | 275.2 | 107.4 | 60.8 | 121.4 |
| Sm | 31.8 | 28.4 | 44.4 | 18.8 | 9.3 | 24.4 |
| Eu | 8.2 | 7.5 | 11.9 | 5.1 | 2.2 | 7.4 |
| Gd | 20.2 | 20.5 | 32.7 | 12.7 | 6.0 | 17.4 |
| Tb | 2.3 | 2.7 | 3.7 | 1.5 | 0.7 | 2.2 |
| Dy | 11.6 | 13.8 | 18.6 | 6.9 | 3.7 | 10.9 |
| Ho | 1.6 | 2.1 | 2.6 | 1.0 | 0.6 | 1.6 |
| Er | 4.7 | 5.9 | 7.1 | 3.1 | 1.8 | 4.4 |
| Tm | 0.4 | 0.7 | 0.7 | 0.3 | 0.2 | 0.5 |
| Yb | 2.8 | 4.3 | 4.7 | 2.2 | 1.6 | 3.2 |
| Lu | 0.4 | 0.6 | 0.7 | 0.3 | 0.2 | 0.5 |
| Y | 44.16 | 72.33 | 87.86 | 29.48 | 19.57 | 32.43 |
| ΣLREE | 1120.8 | 870.1 | 1182.9 | 678.5 | 372.7 | 675.3 |
| ΣHREE | 88.2 | 122.9 | 158.7 | 57.5 | 34.4 | 73.1 |
| L/H | 12.7 | 7.1 | 7.5 | 11.8 | 10.8 | 9.2 |
| δEu | 0.92 | 0.91 | 0.92 | 0.95 | 0.86 | 1.04 |
| δCe | 0.96 | 0.63 | 0.87 | 0.92 | 0.73 | 0.86 |
| (La/Sm) _N | 5.58 | 6.22 | 4.04 | 6.26 | 8.07 | 4.70 |
| (Gd/Yb) _N | 5.78 | 3.84 | 5.62 | 4.64 | 3.10 | 4.34 |
| (La/Yb) _N | 67.32 | 43.94 | 40.85 | 57.20 | 51.19 | 37.87 |

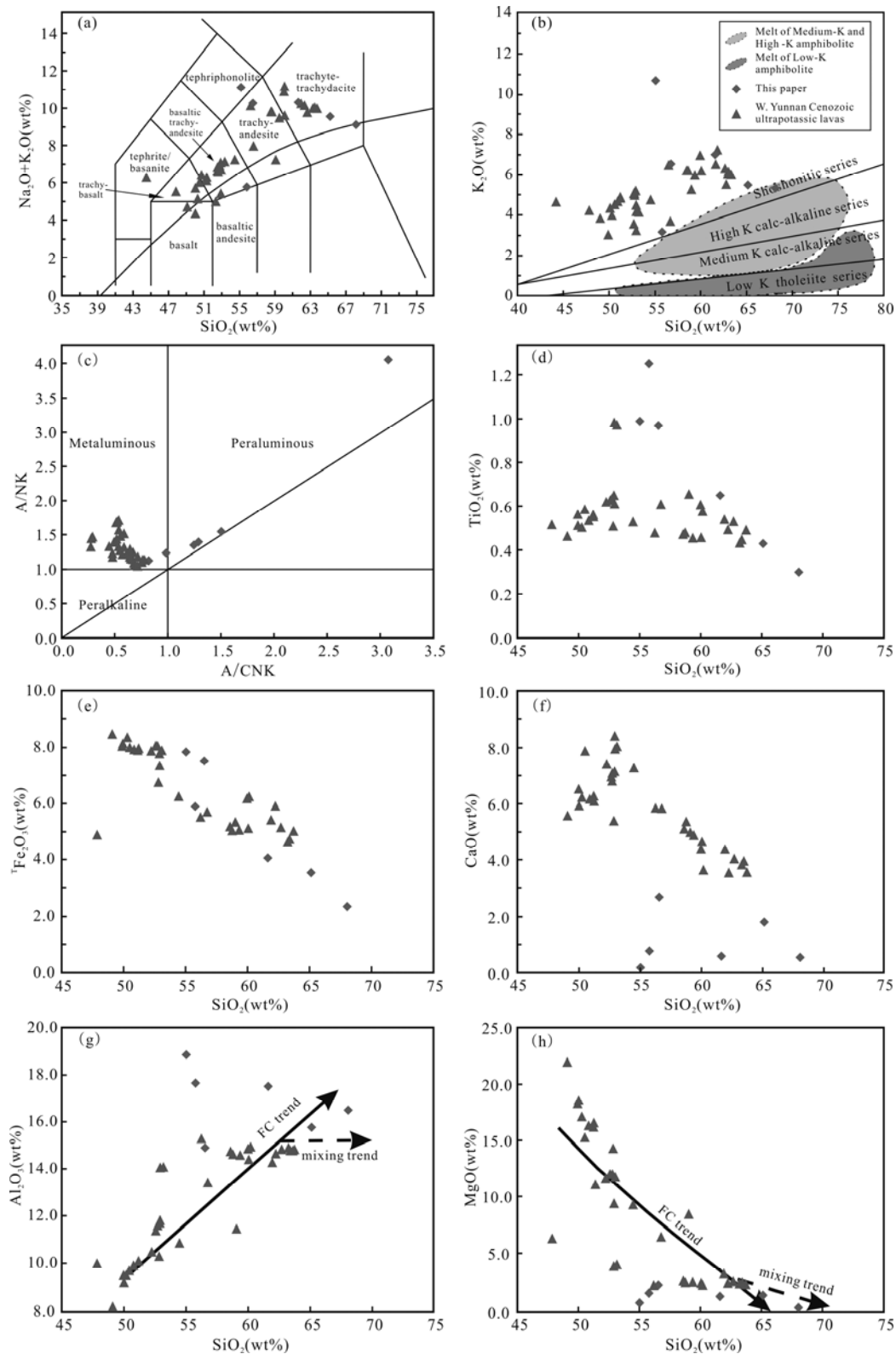


Fig. 6. Geochemical classification and variation of western Yunnan Cenozoic ultrapotassic lavas and Laojiezi alkaline volcanic rocks, western Yangtze craton.

(a), Whole-rock TAS diagram (modified from Middlemost, 1994); (b), K_2O vs SiO_2 diagram (modified from Peccerillo and Taylor, 1976, and Gill, 1981). The shaded fields represent experimental melts of low K amphibolites at 0.6 to 3.2 GPa and 795°C to 1150°C (Rapp et al., 1991; Winter and Newton, 1991; Wolf and Wyllie, 1994; Rapp and Watson, 1995; Winter, 1996), of medium K and high K amphibolites at 0.7 to 3.2 GPa and 825°C to 1150°C (Rapp et al., 1991; Rushmer, 1991, 1993; Sen and Dunn, 1994; Rapp and Watson, 1995; Sisson et al., 2005; Xiong et al., 2005; Xiao and Clemens, 2007), respectively; (c), A/CNK vs A/NK [molar ratio $\text{Al}_2\text{O}_3/(\text{CaO}+\text{Na}_2\text{O}+\text{K}_2\text{O})$ vs $\text{Al}_2\text{O}_3/(\text{Na}_2\text{O}+\text{K}_2\text{O})$]; (d-h), Harker variation diagrams, long black arrows in (g) and (h) highlight the fractional crystallization (FC) trends, dashed black arrows in (g) and (h) indicates a magma mixing trend. The date of western Yunnan Cenozoic ultrapotassic lavas is from Huang et al., 2007.

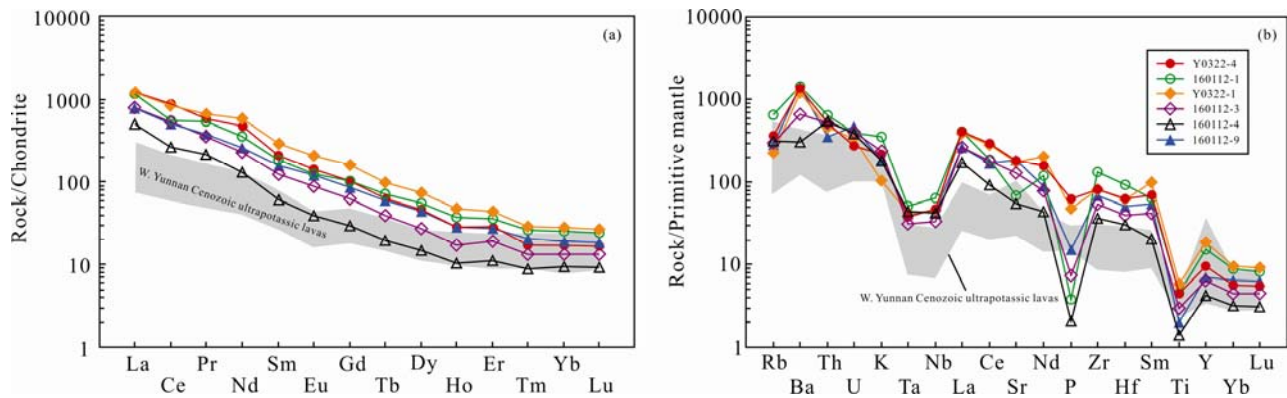


Fig. 7. Chondrite-normalized REE patterns (a) and primitive mantle-normalized diagram (b) of the Laojiezi alkaline volcanic rocks, western Yangtze craton (normalization values from Sun and McDonough, 1989).

Table 3 The analytical results of Sr-Nd isotope of whole rocks

| Spot | $^{87}\text{Rb}/^{86}\text{Sr}$ | $^{87}\text{Sr}/^{86}\text{Sr}$ | I_{Sr} | $^{147}\text{Sm}/^{144}\text{Nd}$ | $^{143}\text{Nd}/^{144}\text{Nd}$ | I_{Nd} | $\varepsilon_{\text{Nd}}(0)$ | $\varepsilon_{\text{Nd}}(t)$ | 2σ | T_{DM1} | T_{DM2} |
|----------|---------------------------------|---------------------------------|-----------------|-----------------------------------|-----------------------------------|-----------------|------------------------------|------------------------------|-----------|------------------|------------------|
| Y0322-4 | 0.23164 | 0.70967 | 0.70956 | 0.11483 | 0.51198 | 0.51196 | -12.80 | -12.45 | 0.19347 | 1799 | 1857 |
| 160112-1 | 1.06470 | 0.71066 | 0.71013 | 0.14201 | 0.51201 | 0.51198 | -12.22 | -11.99 | 0.23669 | 2415 | 1820 |
| Y0322-1 | 0.14514 | 0.70962 | 0.70955 | 0.11598 | 0.51200 | 0.51198 | -12.36 | -12.02 | 0.28483 | 1786 | 1823 |
| 160112-3 | 0.27035 | 0.70853 | 0.70839 | 0.13166 | 0.51210 | 0.51207 | -10.43 | -10.16 | 0.23847 | 1943 | 1671 |
| 160112-4 | 0.67019 | 0.70907 | 0.70874 | 0.11301 | 0.51205 | 0.51203 | -11.43 | -11.08 | 0.23909 | 1662 | 1746 |
| 160112-9 | 0.17905 | 0.70974 | 0.70965 | 0.16454 | 0.51201 | 0.51197 | -12.29 | -12.15 | 0.19049 | 3521 | 1833 |

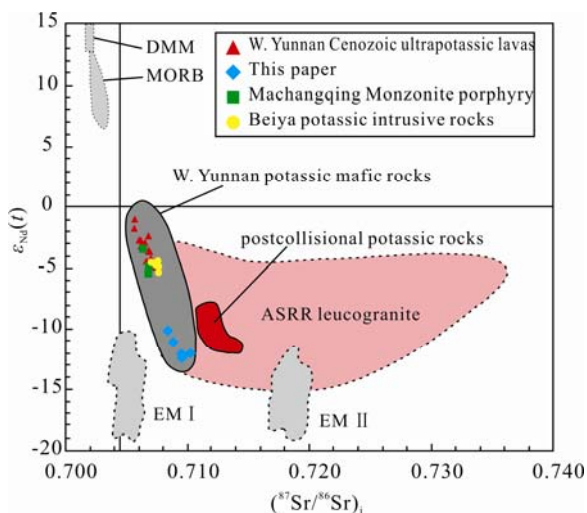


Fig. 8. Variation of $(^{87}\text{Sr}/^{86}\text{Sr})_i$ vs $\varepsilon_{\text{Nd}}(t)$ for the Laojiezi alkaline volcanic rocks, western Yangtze craton.

The field for western Yunnan potassic mafic rocks is from Xu et al., (2001), Li et al., (2002), Guo et al., (2005), and Huang et al., (2010). The field for leucogranite within the Ailao shan-Red River shear zone (ASRR) in western Yunnan is from Zhang & Schärer (1999). The mantle source reservoirs DMM, MORB, EM I and EM II are from Zindler and Hart (1986).

average value of 0.42685. The $^{87}\text{Sr}/^{86}\text{Sr}$ ratios varied from 0.70853 to 0.71066, with an average value of 0.70955, which was higher than the present value of the primitive mantle (0.7045, Depaolo and Wasserburg, 2013). The $^{147}\text{Sm}/^{144}\text{Nd}$ ratios varied from 0.11301 to 0.16454, with an average value of 0.13034, and the $^{143}\text{Nd}/^{144}\text{Nd}$ ratios varied from 0.51198 to 0.51210, with an average value of 0.51203, which was lower than the present value of the primitive mantle (0.512638, Jacobson and Wasserburg,

1980). The volcanic rock samples had higher Sr and lower Nd isotopic compositions, which were characterized by relatively high I_{Sr} (initial $^{87}\text{Sr}/^{86}\text{Sr}$) ratios from 0.70839 to 0.71013 and strongly negative $\varepsilon_{\text{Nd}}(t)$ values from -10.16 to -12.45 (Table 3, Fig. 8). The two-stage Nd isotope-depleted mantle model ages (T_{DM2}) ranged from 1.67 to 1.85 Ga (Table 3).

5.3 Zircon Hf-O isotopes

The results of the in situ zircon Hf-O isotopic analyses are listed in Table 4. Representative zircon CL images are presented in Fig. 9, and the Hf-O isotope variations are presented in Figs. 10–11. The measured zircon $\delta^{18}\text{O}$ values of the trachytic tuff with breccia (Y0322-1) ranged from 5.71‰ to 8.54‰, with an average value of 6.89‰; this sample had a standard deviation of 0.84‰ and internal precision of 0.18‰ to 0.41‰. The $\delta^{18}\text{O}$ values were higher than those of mantle zircon ($(5.3\pm 0.3)\%$, Valley et al., 2005); in particular, the $\delta^{18}\text{O}$ values of seven analysis points were higher than 6.5‰, while another four analysis points had $\delta^{18}\text{O}$ values from 5.3‰ to 6.5‰. The measured zircon $\delta^{18}\text{O}$ values of the trachytic ignimbrite (Y0322-4) ranged from 5.69‰ to 7.28‰, with an average value of 6.71‰; this sample had a standard deviation of 0.44‰ and internal precision of 0.15‰ to 0.42‰. The $\delta^{18}\text{O}$ values were higher than those of mantle zircon; in particular, the $\delta^{18}\text{O}$ values of eight analysis points were higher than 6.5‰, while another three analysis points had $\delta^{18}\text{O}$ values from 5.3‰ to 6.5‰.

The $^{176}\text{Hf}/^{177}\text{Hf}$ ratios of the trachytic tuff with breccia (Y0322-1) ranged from 0.282198 to 0.282559; this sample

Table 4 The analytical results of the zircon Hf-O isotope on Y0322-1 and Y0322-4

| Spot | age(Ma) | $^{176}\text{Lu}/^{177}\text{Hf}$ | $^{176}\text{Hf}/^{177}\text{Hf}$ | 2σ | $\epsilon_{\text{Hf}}(0)$ | $\epsilon_{\text{Hf}}(t)$ | T_{DM1} | T_{DM2} | $f_{\text{Lu/Hf}}$ | $\delta^{18}\text{O}(\text{‰})$ | error |
|----------------|---------|-----------------------------------|-----------------------------------|-----------|---------------------------|---------------------------|------------------|------------------|--------------------|---------------------------------|-------|
| Y0322-1 | | | | | | | | | | | |
| 1 | 33.13 | 0.001058 | 0.282359 | 0.000025 | -14.6 | -13.898 | 1263 | 1709 | -0.96813 | 7.28 | 0.25 |
| 2 | 34.15 | 0.000885 | 0.282532 | 0.000024 | -8.5 | -7.575 | 1015 | 1378 | -0.97334 | 6.81 | 0.23 |
| 3 | 32.40 | 0.000746 | 0.282559 | 0.000024 | -7.5 | -6.835 | 974 | 1326 | -0.97752 | 8.54 | 0.33 |
| 4 | 33.10 | 0.001485 | 0.282418 | 0.000030 | -12.5 | -11.840 | 1194 | 1598 | -0.95526 | 7.93 | 0.25 |
| 5 | 33.76 | 0.001121 | 0.282517 | 0.000025 | -9.0 | -8.290 | 1042 | 1406 | -0.96624 | 7.08 | 0.22 |
| 6 | 34.09 | 0.001398 | 0.282198 | 0.000024 | -20.3 | -19.574 | 1501 | 2015 | -0.95789 | 6.10 | 0.36 |
| 7 | 33.24 | 0.000865 | 0.282543 | 0.000028 | -8.1 | -7.393 | 1000 | 1357 | -0.97396 | 6.48 | 0.29 |
| 8 | 33.34 | 0.001246 | 0.282589 | 0.000038 | -6.5 | -5.764 | 944 | 1269 | -0.96247 | 6.98 | 0.21 |
| 9 | 34.06 | 0.000920 | 0.282506 | 0.000026 | -9.4 | -8.695 | 1053 | 1428 | -0.97228 | 5.95 | 0.41 |
| 10 | 34.07 | 0.000885 | 0.282462 | 0.000024 | -11.0 | -10.242 | 1114 | 1512 | -0.97335 | 6.94 | 0.18 |
| 11 | 34.63 | 0.000707 | 0.282496 | 0.000025 | -9.8 | -9.008 | 1060 | 1446 | -0.97870 | 5.71 | 0.26 |
| Y0322-4 | | | | | | | | | | | |
| 1 | 35.40 | 0.000668 | 0.282384 | 0.000026 | -13.7 | -12.977 | 1216 | 1661 | -0.97988 | 6.74 | 0.20 |
| 2 | 34.05 | 0.000956 | 0.282537 | 0.000023 | -8.3 | -7.574 | 1010 | 1368 | -0.97121 | 6.67 | 0.15 |
| 3 | 32.90 | 0.001708 | 0.282506 | 0.000034 | -9.4 | -8.718 | 1075 | 1428 | -0.94854 | 6.76 | 0.24 |
| 4 | 33.04 | 0.000633 | 0.282524 | 0.000025 | -8.8 | -8.048 | 1019 | 1393 | -0.98094 | 6.83 | 0.37 |
| 5 | 32.50 | 0.000809 | 0.282481 | 0.000030 | -10.3 | -9.582 | 1084 | 1475 | -0.97563 | 6.48 | 0.17 |
| 6 | 33.69 | 0.001292 | 0.282525 | 0.000023 | -8.7 | -8.021 | 1036 | 1391 | -0.96107 | 6.33 | 0.42 |
| 7 | 33.67 | 0.001022 | 0.282383 | 0.000026 | -13.8 | -13.048 | 1228 | 1664 | -0.96922 | 6.86 | 0.34 |
| 8 | 35.90 | 0.001336 | 0.282425 | 0.000030 | -12.3 | -11.520 | 1179 | 1583 | -0.95977 | 7.28 | 0.26 |
| 9 | 33.44 | 0.001000 | 0.282439 | 0.000030 | -11.8 | -11.049 | 1148 | 1555 | -0.96988 | 7.08 | 0.32 |
| 10 | 32.63 | 0.000977 | 0.282412 | 0.000050 | -12.7 | -12.029 | 1186 | 1608 | -0.97057 | 7.10 | 0.21 |
| 11 | 33.16 | 0.000797 | 0.282405 | 0.000026 | -13.0 | -12.260 | 1190 | 1621 | -0.97599 | 5.69 | 0.21 |

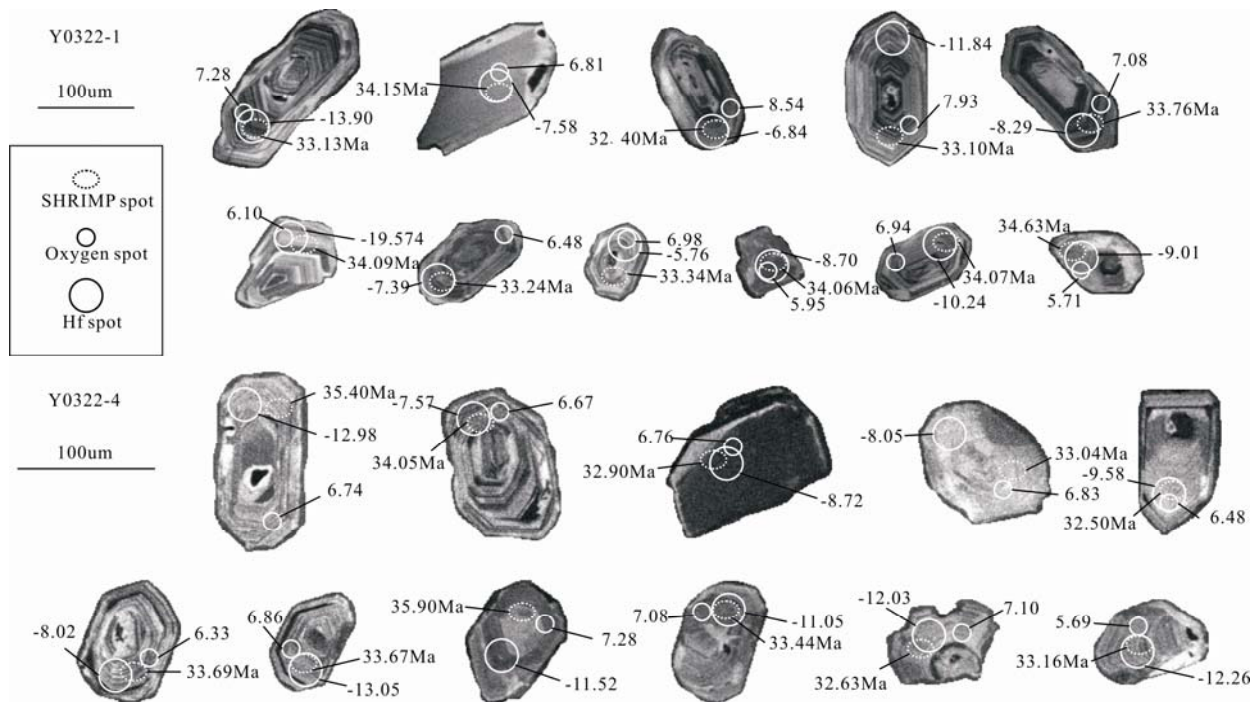


Fig. 9. Cathodoluminescence images of representative analyzed zircons with SHRIMP U-Pb, O, and LA-MC-ICP-MS Hf isotope date for the Laojiezi alkaline volcanic rocks, western Yangtze craton.

had strongly negative ϵ_{Hf} values (-19.574 to -5.768), with an average value of -9.92, and the two-stage Hf depleted mantle-model ages (T_{DM2}) ranged from 2.0 to 1.3 Ga, with an average value of 1.5 Ga. The $^{176}\text{Hf}/^{177}\text{Hf}$ ratios of tetrachytic ignimbrite (Y0322-4) ranged from 0.282383 to 0.282537; this sample had strongly negative ϵ_{Hf} values (-13.048 to -7.574), with an average value of -10.44, and the two-stage Hf depleted mantle-model ages (T_{DM2}) ranged from 1.4 to 1.7 Ga, with an average value of 1.5 Ga

(Table 4).

6 Discussions

6.1 Geochronology

Most of the previously published age data from the Laojiezi alkaline volcano-magmatic complex included K-Ar isotope and U-Pb ages. Zhang Yuquan et al. (1997) were the first to report that a trachyte at Laojiezi yielded a

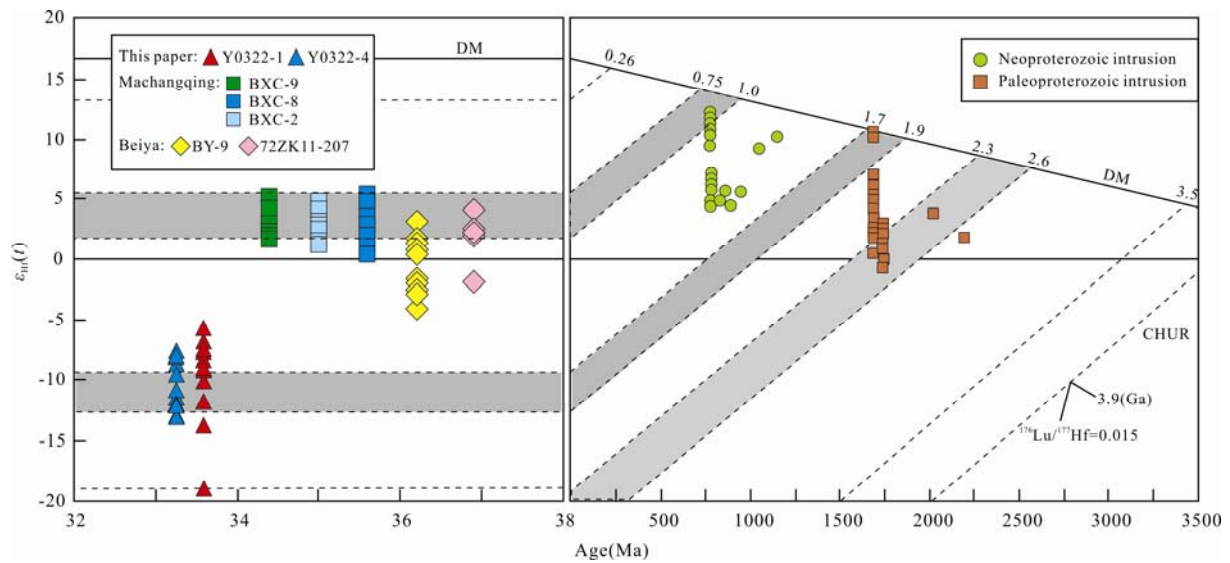


Fig. 10. Variation of initial ϵ_{Hf} isotope values vs. zircons U-Pb ages.

The date for zircons from the western Yangtze craton are plotted for comparison and included Machangqing and Beiya intrusion (Lu et al., 2013), Paleoproterozoic intrusion (Zhao et al., 2010), and Neoproterozoic intrusion (Huang et al., 2008, 2009). Abbreviations: CHUR=chondrite uniform reservoir, DM=depleted mantle. The light gray fields represent episodes of major juvenile crustal growth in the Yangtze craton (Sun et al., 2009; Zhao et al., 2010; Wang et al., 2012).

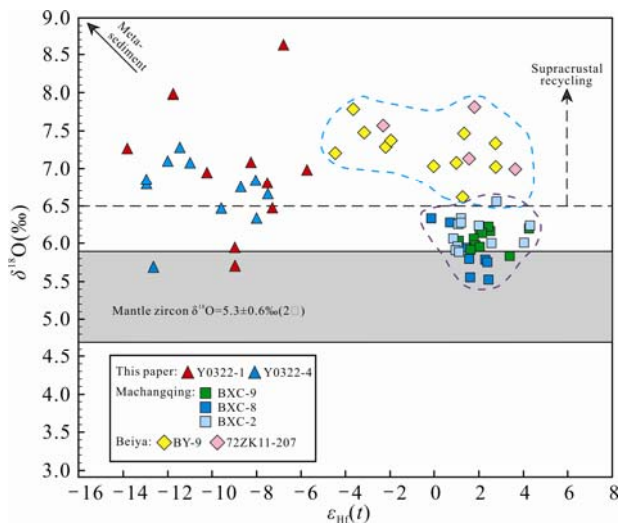


Fig. 11. Combined zircon Hf-O isotope diagram for the Laojiezi alkaline volcanic rocks, western Yangtze craton.

The light gray band represents the range of igneous zircons in high-temperature equilibrium with the mantle ($\delta^{18}\text{O}=5.3\pm 0.6\text{‰}$, 2σ ; Valley et al., 1998, 2005). The zircon Hf-O date from Machangqing and Beiya (Lu et al., 2013) are plotted for comparison. Zircon $\delta^{18}\text{O}>6.5\text{‰}$ indicates significant incorporation of supracrustal material.

biotite K-Ar isotope age of 33.51 ± 1.9 Ma. Lu et al. (2012) obtained a SHRIMP zircon U-Pb age of 33.4 ± 0.3 Ma for alkaline porphyry, whereas the (U-Th)/He zircon dating of the same porphyry yielded a similar age of 33.4 ± 1.6 Ma. In addition, a lamprophyre from Laojiezi yielded a phlogopite $^{40}\text{Ar}/^{39}\text{Ar}$ age of 33.7 ± 0.5 Ma (Lu et al., 2015). Sun Chundi et al. (2017) reported an LA-ICPMS U-Pb age of 34.1 ± 0.3 Ma for pseudoleucite porphyry. Yan Qinggao et al. (2017) reported SHRIMP U-Pb ages of 33.63 ± 0.5 Ma and 33.27 ± 0.38 Ma for alkaline trachytic tuff and

ignimbrite (Fig. 12), respectively. All these ages clearly indicated that the multistage emplacement of the Laojiezi alkaline intrusions occurred within a very short period and that the magmatism of the Laojiezi sector occurred during the Oligocene.

Previous studies suggested that the alkaline porphyry belt was closely related to the large-scale strike-slip Jinshajiang-Ailaoshan shear zone, which deeply cut the lithosphere over space and time. From north to south in this belt, the shear zone produced the Yulong Cu-Mo polymetallic deposit (40 Ma to 38 Ma), Mangzong Cu-Fe polymetallic deposit (41 Ma to 34 Ma), Duoxiasongduo Cu-Mo polymetallic deposit (37.5 Ma), Lujiacun Cu-Au polymetallic deposit (36.2 Ma), Luobudi Cu-Au deposit (32.27 Ma), Zhiju Cu-polymetallic deposit (31.28 Ma), Beiya Au-polymetallic deposit (36.9 Ma to 34.6 Ma), Machangqing Cu-Mo(Au) polymetallic deposit (35.6 Ma to 34.8 Ma), and Tongchang Cu-Mo polymetallic deposit (34.4 Ma), which comprise a thousand-mile-long tectonic-magmatic-hydrothermal polymetallic mineralized zone (Fig. 1) (Hou Zengqian et al., 2003; Wang Denghong et al., 2004; Bi Xianwu et al., 2005; Liang et al., 2007; Liang Huaying et al., 2004, 2009; Xue Chuandong et al., 2010; Li Wenchang et al., 2010; Lu et al., 2012; Deng Jun et al., 2010, 2014; Tang Juxing et al., 2017; Jiang Xiaojun et al., 2018).

The Laojiezi complex is an important component of the alkaline porphyry belt, which is coeval with the Beiya and Machangqing sectors in the adjacent region of the western Yangtze craton. This synchronicity between the Laojiezi, Machangqing and Beiya magmatism suggests that the

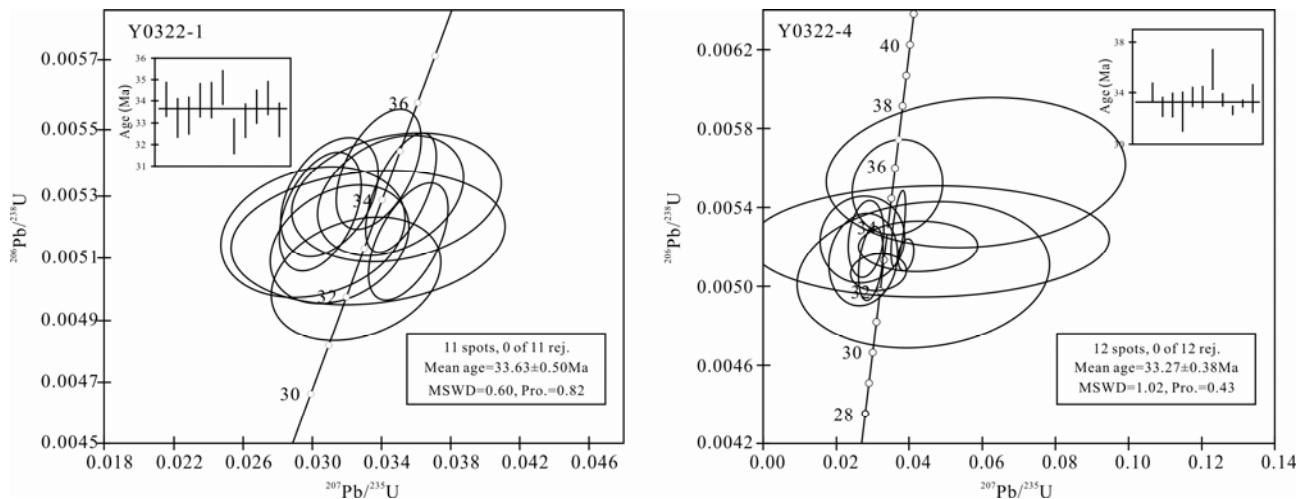


Fig. 12. SHRIMP U-Pb concordia diagrams of the Laojiezi alkaline volcanic rocks (after Yan Qinggao et al., 2017).

same tectonic setting existed during regional magmatism, which was triggered when the tectonic regime changed after the Indian-Asian continent-continent collision (40–26 Ma, Hou Zengqian et al., 2006).

6.2 Material sources

The major- and trace-element data showed that the alkaline volcanic rocks were enriched in large-ion lithophile elements (LILE) and light rare earth elements (LREE) but depleted in heavy rare earth elements (HREE) and high-field-strength elements (HFSE); these rocks were characterized by right-deviated chondrite-normalized rare-earth-elemental distribution curves, which were similar to those of continental tholeiite. These geochemical signatures suggest that the material sources may have originated from the partial melting of thickened lower crust and upper mantle or the partial melting of enriched lithospheric mantle that was metasomatized by slab-derived fluid/melt (He et al., 2013; Lu et al., 2013b).

The rocks had Rb/Sr values from 0.04 to 0.28, with an average value of 0.11, which was much higher than the average mantle value of 0.034 (Taylor et al., 1985); Th/La values from 0.13 to 0.38, with an average value of 0.21, which was close to the average value of continental crust but different from the average mantle value of 0.125 (Weaver et al., 1991); and Th/Nb values from 0.95 to 1.85, with an average value of 1.34, which was much higher than the average mantle value of 0.18 (Saunders et al., 1988). In addition, the samples had higher SiO₂ and Al₂O₃ contents and lower Mg[#] values (Tables 1–2), which were important signs of crustal components. According to the above data, the compositional variations and elemental correlations on Harker diagrams (Fig. 6) indicated that the Laojiezi alkaline volcanic rocks may have originated from the partial melting of continental crust.

Crustal components are enriched in such elements as Sr,

Pb, and Zr, and have higher SiO₂ contents but low ϵ_{Nd} values, so mixing between mantle-derived magma and upper crustal material generates a clearly negative correlation between ϵ_{Nd} and SiO₂ (Jahn et al., 1999). However, the observed ϵ_{Nd} values were not clearly negative with increasing SiO₂ (Fig. 13b), while a very weak correlation existed between Nd(*t*) and 100/*w*(Nd) (Fig. 13d), suggesting a very low degree of contamination during ascent through the crust, which was also evidenced in the FC models of major elements (Figs. 6g–h). Furthermore, the higher initial Sr isotope values (0.70839 to 0.71013) and lower ϵ_{Nd} values (–12.45 to –10.16) indicated that a crustal component was involved in the generation of the alkaline volcanic rocks, which was also supported by their high concentrations of Zr (418.7–1505.2 ppm), Pb (69.1–374.7 ppm), Th (30.8–57.5 ppm) and U (5.9–9.8 ppm). Moreover, the Nd two-stage model ages T_{DM2} (1.86–1.67 Ga, Table 4) indicated that the crustal component of the Laojiezi alkaline volcanic rocks may have originated from the melting of Paleoproterozoic crustal materials.

The zircon Hf–O isotopic compositions showed that the $\delta^{18}\text{O}$ values of these rocks were higher than the $\delta^{18}\text{O}$ values of mantle zircon (5.3±0.3)‰, and their low ϵ_{Hf} values fell within the field of the crust. Both Hf–O isotopic values had a wide range of variation (Table 4, Figs. 10–11), which did not reflect a single source of material. On the $\delta^{18}\text{O}$ – ϵ_{Hf} diagram, two analysis points fell within the mantle zircon field, suggesting that their magmatic materials may have contained minor residual continental lithospheric mantle. The presence of minor analysis points with high $\delta^{18}\text{O}$ values, which plotted close to the supracrustal metasediment field, suggested that some rocks were contaminated by upper crustal materials (Fig. 11).

Hong Tao et al. (2015) determined that a 1.8 Ga- to 2.5

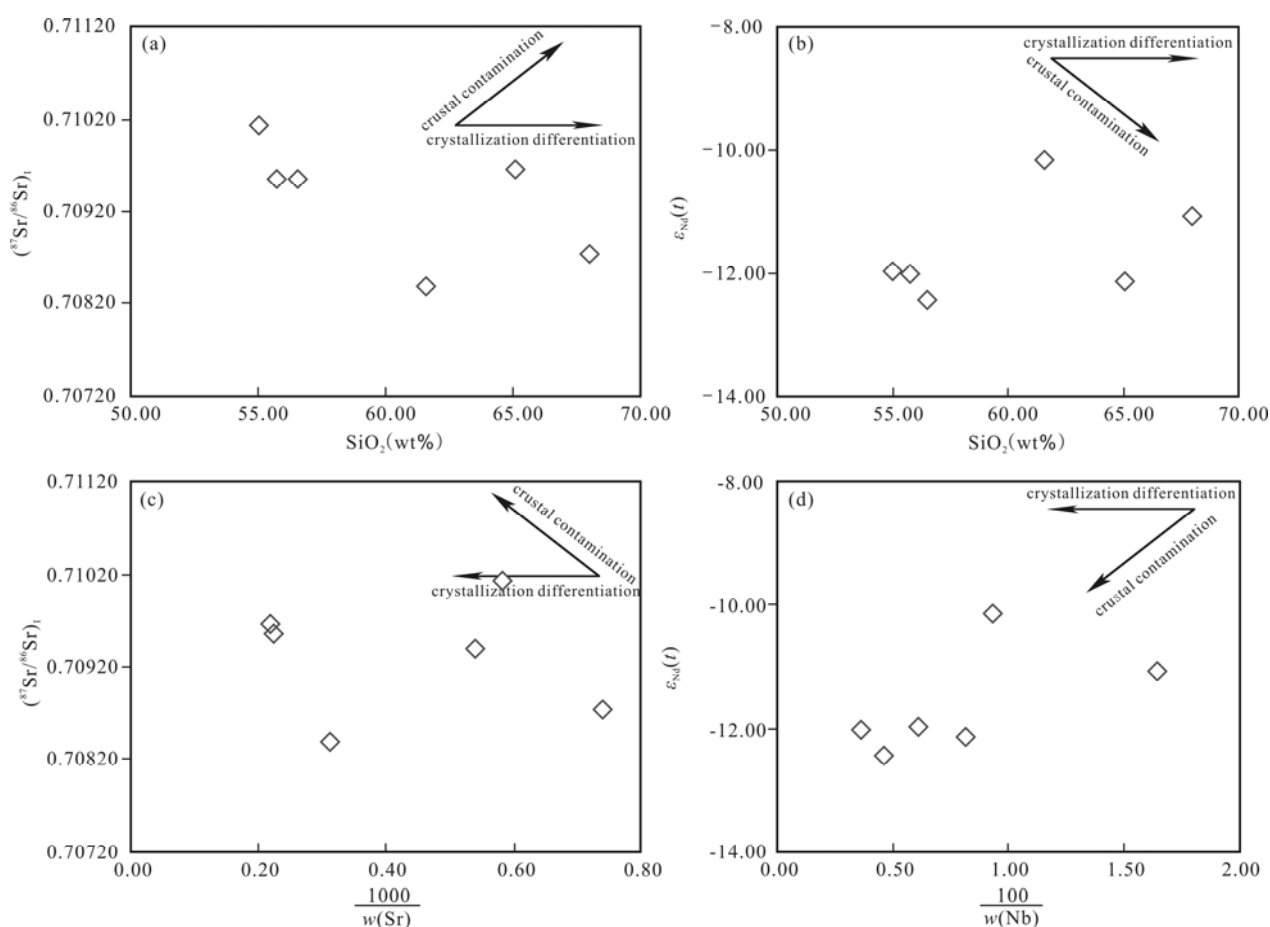


Fig. 13. Diagrams of the Sr, Nd, SiO_2 for Laojiezi alkaline volcanic rocks, western Yangtze craton.

Ga-old basement existed along the western margin of the Yangtze craton, which underwent two major magmatic formation events from 1.85 to 1.7 Ga and from 891 to 167 Ma based on ages from inherited zircons with sub-rounded shapes in granite porphyry. Lu et al. (2013b) studied the zircon Hf-O isotopes of the Beiya felsic intrusion and Machangqing granite intrusion, which are located near the Jinshajiang-Ailaoshan suture (Figs. 10–11); these authors proposed that the Machangqing granite intrusion was derived from the partial melting of a Neoproterozoic intracrustal amphibolitic source (with positive zircon ϵ_{Hf} (0.3–4.7) values, 1.1- to 0.8-Ga depleted Hf mantle-model ages and mantle-like zircon $\delta^{18}\text{O}$ values (5.53–6.35‰)). The Beiya felsic intrusions were derived from the partial melting of a K-rich mafic source that had mixed with a metasedimentary component (with variable ϵ_{Hf} (–4 to 4) values, 0.85- to 1.37-Ga depleted Hf mantle-model ages and high zircon $\delta^{18}\text{O}$ values (7.0‰–7.8‰)). In this paper, the two-stage Hf model ages ($T_{\text{DM}2}$) of the trachytic tuff with breccia and trachytic ignimbrite ranged from 2.0 to 1.3 Ga and from 1.7 to 1.4 Ga, respectively, which were consistent with a Paleoproterozoic source that was aligned to the most significant period of juvenile crustal growth in

the Yangtze craton from 1.7 to 1.9 Ga (Fig. 10, Table 4) (Sun et al., 2009; Wang et al., 2012). Compared to the ϵ_{Hf} and $\delta^{18}\text{O}$ values of the Beiya and Machangqing rocks, the Laojiezi alkaline volcanic rocks had a wide range of variation for the ϵ_{Hf} and $\delta^{18}\text{O}$ values (ϵ_{Hf} = –19.57 to –5.764, $\delta^{18}\text{O}$ = 5.69–7.93; Table 4, Figs. 10–11), indicating that a heterogeneous source was involved during the magma genesis of the Laojiezi alkaline volcanic rocks.

Therefore, the Laojiezi alkaline volcanic rocks originated from the partial melting of Paleoproterozoic to Mesoproterozoic lower crust with minor residual CLM and supracrustal metasediments.

6.3 Fractional and evolutionary processes

The average zircon $\delta^{18}\text{O}$ values of the Laojiezi alkaline volcanic rocks were $6.95 \pm 0.47\text{‰}$ (sample Y0322-1) and $6.66 \pm 0.29\text{‰}$ (sample Y0322-4). These values suggested continental crust components, which were also indicated by the zircon ϵ_{Hf} values (–19.574 to –5.764 for sample Y0322-1 and –13.048 to –7.574 for sample Y0322-4) (Figs. 10–11, Table 4). However, a small amount of $\delta^{18}\text{O}$ values fell within the field of mantle zircon, suggesting that their magmatic materials may have contained minor

residual CLM.

Weakly positive or negative correlations existed between the Sr and Nd isotopic compositions and between the Sr and Nd contents vs. SiO₂ contents (Fig. 13). Furthermore, the similar and limited variations in the Sr-Nd isotopic ratios (Table 3) suggested that minor shallow crustal contamination existed during rock formation, which was also indicated by the minor higher δ¹⁸O values and slight magma-mixing trend (Figs. 6g–h).

As mentioned above, the Laojiezi alkaline volcanic rocks were mainly derived from the partial melting of lower crust with minor residual CLM and supracrustal metasediments. Consequently, the negative correlations among TiO₂, ¹Fe₂O₃, CaO, and SiO₂ suggested that the alkaline volcanic rocks likely originated from fractional crystallization during the evolution of the magmas (Figs. 6d–f). Moreover, the pronounced depletions in Ta, Nb, Sr, P, and Ti (Fig. 7b) further demonstrated that fractional crystallization occurred during the formation of these volcanic rocks. The negative correlation between ¹Fe₂O₃ and SiO₂ indicated the separation of mafic minerals during the evolution of these magmas. In addition, minor potassic feldspar fractionation may have occurred in these volcanic rocks, as indicated by the negative correlations between K₂O and SiO₂ (Fig. 6a) and between Ba and SiO₂ (not shown). The depletions in Ti, Ta, and Nb may have resulted from the separation of ilmenite and titanite, whereas the depletion in P resulted from the separation of apatite.

In addition, similar variations existed in the chondrite-normalized REE patterns, primitive mantle-normalized trace element patterns, and Harker variation diagrams for the western Yunnan potassic mafic lavas and Laojiezi alkaline volcanic rocks, suggesting that these rocks formed in similar tectonic settings. However, the differences in their LREE contents, (⁸⁷Sr/⁸⁶Sr)_i vs. ε_{Nd} values and zircon δ¹⁸O vs. ε_{Hf} values indicated that these rocks may have experienced different fractional-crystallization processes. The Laojiezi alkaline volcanic rocks may have experienced more intensive magmatic evolution and differentiation, as demonstrated by their higher LREE contents and lower Fe, Mg, Ca, Ti and P contents (Figs. 7–8, Table 2).

In general, the same tectonic setting existed between the Laojiezi region and the western Yunnan margin, although these areas had different material sources and/or magmatic evolutions. The larger range of variations for the Sr-Nd-Hf-O isotopic components and higher LREE contents probably indicate the greater involvement of lower crustal components and higher degrees of magmatic evolution and differentiation during the magma genesis of the Laojiezi lavas.

6.4 Tectonic implications

The western Yunnan ultrapotassic lavas formed within a continental post-collision arc (CAP+PAP) and the Laojiezi alkaline volcanic rocks from the western Yangtze craton formed in a within-plate setting (WIP) (Fig. 14). However, the similar geochemical variations (Figs. 6–7), coeval nature and close spatial relationships between the Laojiezi, Machangqing and Beiya sectors suggested that these rocks were controlled by the same tectonic evolution processes. Lu et al. (2013a) reported that the Machangqing granite intrusion and Beiya felsic intrusion near the Jinshajiang-Ailaoshan suture were derived from the partial melting of a Neoproterozoic intracrustal amphibolitic source and a K-rich mafic source that had mixed with a metasedimentary component, respectively. As mentioned above, the Laojiezi alkaline volcanic rocks likely originated from the partial melting of thickened lower crust and became mixed with minor residual CLM and an upper crustal metasedimentary component.

Liu Futian et al. (2000) and Lei et al. (2009) reported a ~300-km-wide mantle diapir that originated from a depth of ~450 km beneath western Yunnan based on geophysical data. Clemens (2003) proposed a plausible mechanism for inducing both lower-crustal melting and CLM melting, i.e., asthenospheric upwelling that was induced by the thinning of lithospheric mantle. Therefore, we propose that alkaline magmatism occurred in response to the removal of overthickened CLM beneath the western Yangtze craton following the Indian-Asian continent-continent collision, which occurred at 41–31 Ma (Fig. 15a).

In this model, the convectively removed CLM beneath

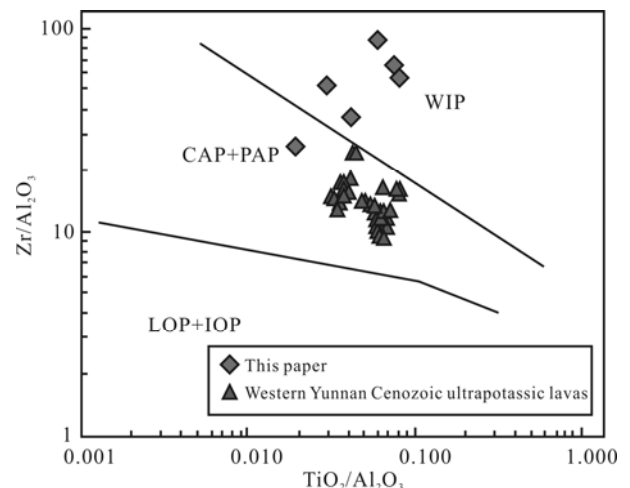


Fig. 14. Discrimination diagrams of tectonic settings of Laojiezi alkaline volcanic rocks, western Yangtze craton (modified from Muller et al., 1992).

The date of western Yunnan Cenozoic ultrapotassic lavas is from Huang Xiaolong et al., 2007. WIP, Within-Plate; CAP, Continental Arc; PAP, Postcollisional Arc; LOP, Late Oceanic Arc; IOP, Initial Oceanic Arc.

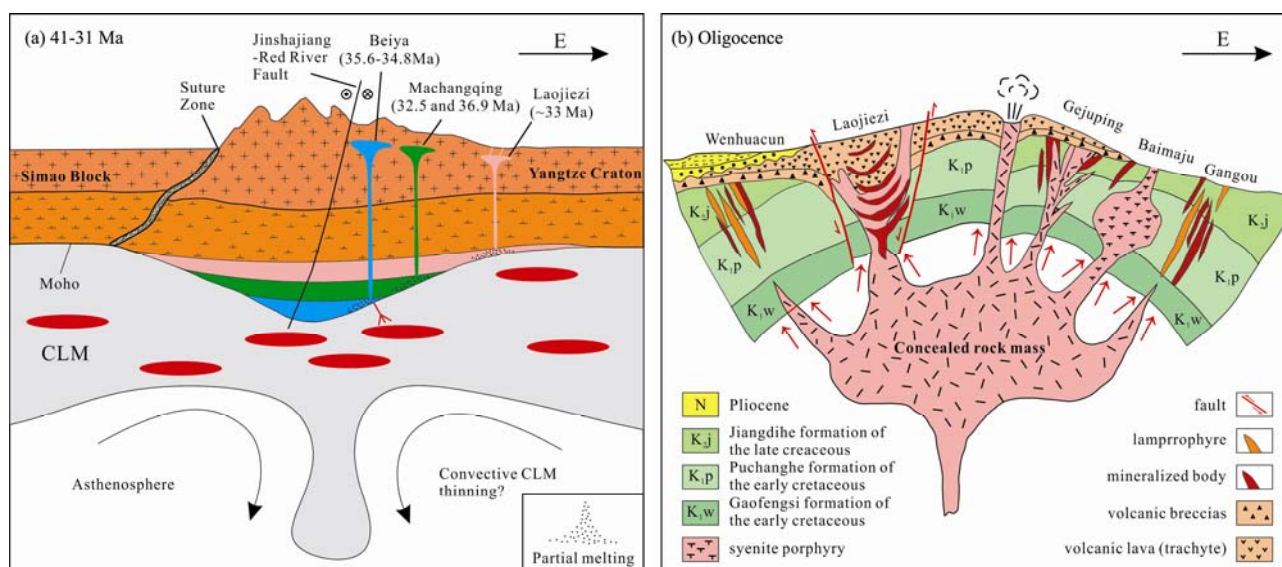


Fig. 15. The diagenetic model for the formation of western Yangtze Craton intracratonic alkaline magmatism.

(a), In the 41-31 Ma, the lower part of the over thickened lithospheric mantle adjacent to suture was possibly convectively removed, which may have led to upwelling of the asthenosphere, partial melting of the lower crust as well as metasomatic veins within residual Yangtze continental lithospheric mantle (CLM) (modified from Lu et al., 2013); (b), In the Oligocene, shallow alkaline intrusion generated with the alkaline magma emplaced along the fracture zone or fissure zone. Alkaline volcanic rocks were formed by part of magma erupted rapidly to the crustal surface from the volcanic vent (modified from Li Guanguodou et al., 2010).

the Yangtze craton from the Indian-Asian continent-continent collision may have induced the upwelling of hot asthenosphere and the melting of mafic magma through the partial melting of CLM. The fractional crystallization of magmatic melt occurred near the Moho in the crust and mantle transition zone because of the melt's higher density, which further resulted in the formation of alkaline basaltic magma through the partial melting of thickened lower crust because of the generation of thermal energy. An intracratonic transition from a compressional to extensional setting occurred in the intraplate region of the western Yangtze craton during the post-collision period, which was caused by changes in the large-scale intracratonic strike-slip tectonic regime following the continued India-Asian continent-continent collision. The alkaline porphyry belt formed near the large-scale ductile left-lateral shear zone, and the magmatic melt migrated along the weak tectonic zone. A shallow magma chamber formed when the magma migrated and was emplaced in the upper crust in the Laojiezi region in the intraplate region of the western Yangtze craton. The fractional crystallization of clinopyroxene, sanidine and Ti-Fe oxides occurred, and minor supracrustal metasediment was mixed in the shallow magma chamber. During the Oligocene, the alkaline intrusions that were generated by the magma were emplaced along the E- to W- or ENE- to WSW-trending tectonic zone, and alkaline volcanic rocks formed after some of the magma rapidly erupted to the surface from the volcanic vent in the Laojiezi region (Fig. 15b).

7 Conclusions

The results of the petrologic, major- and trace-element and isotopic analyses of the Laojiezi alkaline volcanic rocks in the western Yangtze craton enabled us to draw the following conclusions:

(1) A large quantity of U-Pb and K-Ar ages indicated that the magmatism in the Laojiezi sector occurred during the Oligocene, in which multistage emplacement occurred over a very short period. Laojiezi was coeval with the Beiya and Machangqing sectors in the adjacent region of the western Yangtze craton. This suggested that the same tectonic setting existed during the regional magmatism, which was triggered when the tectonic regime changed after the Indian-Asian continent-continent collision.

(2) In situ zircon Hf-O isotopic, whole-rock Sr-Nd isotopic, and major- and trace-element data suggested that the Laojiezi alkaline volcanic rocks originated from the partial melting of Paleoproterozoic to Mesoproterozoic lower crust with minor residual CLM and supracrustal metasediments; these rocks were deposited in the stable continental intraplate region of the Yangtze craton.

(3) The negative correlations among TiO_2 , $^1\text{Fe}_2\text{O}_3$, CaO and SiO_2 and the pronounced depletions in Ta, Nb, Sr, P, and Ti suggested that the Laojiezi alkaline magmas underwent fractional crystallization and minor magma mixing. Furthermore, the larger range of variations for the Sr-Nd-Hf-O isotopic components and higher LREE contents probably indicate the greater involvement of

lower crustal components and higher degrees of magmatic evolution and differentiation during the magma genesis of the Laojieze lavas.

(4) The Laojieze alkaline magmatism occurred in response to the removal of the lower overthickened CLM beneath the western Yangtze craton, which occurred at 41–31 Ma following the Indian-Asian continent-continent collision. During this process, thickened lower crust and minor CLM were partially melted by changes in the large-scale intracontinental strike-slip tectonic regime of the southeastern margin of the Qinghai-Tibetan Plateau, SW China. The alkaline porphyry intrusion was generated with the emplacement of alkaline basaltic magma along the E- to W- or ENE- to WSW-trending tectonic zone, where these materials mixed with minor super crustal metasediment and alkaline volcanic rocks formed from magmas that rapidly erupted to the surface from the volcanic vent in the Laojieze region.

Acknowledgments

This study was funded by the Open Foundation of the Beijing SHRIMP Center (DDC15-016), the Applied Basic Research Program Youth Project of Yunnan Province (2016DF031) and the National Basic Research Program of China (2015CB452605), which are gratefully acknowledged. We thank Longyan Jiang, who is a chief engineer of the Feilong mineral company in Yao'an, for their fieldwork assistance. Xinwei Li and Hong Zhao from the National Research Center for Geoanalysis in Beijing are thanked for their assistance with the major- and trace-element, Sr-Nd isotope and zircon Hf isotope analyses. Linlin Li and Shouye Liu from the Beijing SHRIMP Center (National Science and Technology Infrastructure) are thanked for their technical assistance, such as the sample loading, additional monitoring of instrument performance, and data processing.

Manuscript received Apr. 4, 2018

accepted Jul. 27, 2018

edited by Liu Lian

References

- Bi Xianwu, Hu Ruizong, Pen Jiantang, Wu Kaixin, Su Wenchao and Zhan Xinzhi, 2005. Geochemical characteristics of the Yao'an and Machangqing alkaline-rich intrusions. *Acta Petrologica Sinica*, 21(1): 113–124 (in Chinese with English abstract).
- Blichert-Toft, J., Chauvel, C., and Albarede, F., 1997. Separation of Hf and Lu for high-precision isotope analysis of rock samples by magnetic sector-multiple collector ICP-MS. *Contributions to Mineralogy & Petrology*, 127(3): 248–260.
- Cheng Jin, Xia Bin and Zhang Yuquan, 2007. Petrological and Geochemical characteristics of Yao'an alkaline complex in Yunnan Province. *Geotectonica Et Metallogenia*, 31(1): 118–125 (in Chinese with English abstract).
- Clemens, J.D., 2003. S-type granitic magmas-petrogenetic issues, models and evidence. *Earth-Science Reviews*, 61(1): 1–18.
- Deng Jun, Hou Zengqian Mo Xuanxue, Yang Liqiang, Wang Qingfei and Wang Changmin, 2010. Superimposed orogenesis and metallogenesis in Sanjiang Tethys. *Mineral Deposits*, 29(1): 37–42 (in Chinese with English abstract).
- Deng, J., Wang, Q.F., Li, G.J., and Santosh, M., 2014. Cenozoic tectono-magmatic and metallogenic processes in the Sanjiang region, southwestern China. *Earth-Science Reviews*, 138: 268–299.
- Deng, J., Wang, Q.F., Li, G.J., and Zhao, Y., 2015. Structural control and genesis of the Oligocene Zhenyuan orogenic gold deposit, SW China. *Ore Geology Reviews*, 65: 42–54.
- DePaolo, D.J., and Wasserburg, G.J., 2013. Inferences about magma sources and mantle structure from variations of $^{143}\text{Nd}/^{144}\text{Nd}$. *Geophysical Research Letters*, 3(12): 743–746.
- Elhlou, S., Belousova, E., Griffin, W.L., Pearson, N.J., and O'Reilly, S.Y., 2006. Trace element and isotopic composition of GJ-red zircon standard by laser ablation. *Geochimica Et Cosmochimica Acta*, 70(18): A158–A158.
- Flower, M.F.J., Hoang, N., Lo, C.H., Chi, C.T., Cu'o'ng, N.Q., Liu, F.T., Deng, J.F., and Mo, X.X., 2013. Postassic magma genesis and the Ailao-Shan-Red River fault. *Journal of Geodynamics*, 69(Special Issue): 84–105.
- Griffin, W.L., Pearson, N.J., Belousova, E., Jackson, S.E., Achterbergh, E.V., O'Reilly, S.Y., and Shee, S.R., 2000. The Hf isotope composition of cratonic mantle: LA-MC-ICPMS analysis of zircon metacrysts in kimberlites. *Geochimica Et Cosmochimica Acta*, 64(1): 133–147.
- Griffin, W.J., Wang, X., Jackson, S.E., Pearson, N.J., O'Reilly, S.Y., Xu, X.S., and Zhou, X.M., 2002. Zircon chemistry and magma mixing, SE China: In-situ analysis of Hf isotopes, Tonglu and Pingtan igneous complexes. *Lithos*, 61(3): 237–269.
- Gill, J., 1981. *Orogenic Andesites and Plate Tectonics*. New York: Springer, p. 358.
- Guo, Z.F., Hertogen, J., Liu, J.Q., Pasteels, P., Boven, A., Punzalan, L., He, H.Y., and Luo, X.J., 2005. Potassic magmatism in Western Sichuan and Yunnan Provinces, SE Tibet, China: Petrological and geochemical constraints on petrogenesis. *Journal of Petrology*, 46(1): 33–78.
- Hu, R.Z., Burnard, P.G., Bi, X.W., Zhou, M.F., Pen, J.T., Su, W.C., and Wu, K.X., 2004. Helium and argon isotope geochemistry of alkaline intrusion-associated gold and copper deposits along the Red River–Jinshajiang fault belt, SW China. *Chemical Geology*, 203(3): 305–317.
- Hou, Z.Q., Ma, H.W., Zaw, K., Zhang, Y.Q., Wang, M.J., Wang, Z., Pan, G.T., and Tang, R.L., 2003. The Himalayan Yulong porphyry copper belt: Product of large scale strike-slip faulting in eastern Tibet. *Economic Geology*, 98: 125–145.
- Hou Zengqiang, Pan Guitang, Wang Anjian, Mo Xuanxue, Tian Shihong, Sun Xiaoming, Ding Lin, Wang Erqi, Gao Yongfeng, Xie Yuling, Zeng Pusheng, Qin Kezhang, Xu Jifeng, Qu Xiaoming, Yang Zhiming, Yang Zusen, Fei Hongchai, Meng Xiangjin and Li Zhenqing, 2006. Metallogenesis in Tibetan collisional orogenic belt: II. Mineralization in late-collisional transformation setting. *Mineral Deposits*, 25(5): 521–543 (in Chinese with English abstract).

- abstract).
- Hou, Z.Q., Zaw, K., Pan, G.T., Mo, X.X., Xu, Q., Hu, Y.Z., and Li, X.Z., 2007. Sanjiang Tethyan metallogenesis in S.W. China: Tectonic setting, metallogenic epochs and deposit types. *Ore Geology Reviews*, 31(1): 48–87.
- Hou, Z.Q., Zhou, Y., Wang, R., Zhang, Y.C., He, W.Y., Zhao, M., Noreen, J.E., and Roberto, F.W., 2017. Recycling of metal-fertilized lower continental crust: Origin of non-arc Au-rich porphyry deposits at cratonic edges. *Geology*, 45 (6): 563–566.
- Huang, X.L., Xu, Y.G., Yang, Q.J., and Chen, L.L., 2006. Olivine phenocrysts and spinel inclusions in the Wozhong high-Mg and K-rich lavas from the western Yunnan, China: petrogenesis and geodynamic implications. *Acta Petrologica Sinica*, 22(6), 1553–1564.
- Huang, X.L., Xu, Y.G., Yang, Q.J., and Qiu, H.N., 2007. Geochemistry of late Eocene high-Mg ultrapotassic lavas from western Yunnan, China: Constraints on petrogenesis. *Geochimica*, 36(2), 120–138.
- Huang, X.L., Xu, Y.G., Li, X.H., Li, W.X., Lan, J.B., Zhang, H.H., Liu, Y.S., Wang, Y.B., Li, H.Y., Luo, Z.Y., and Yang, Q.J., 2008. Petrogenesis and tectonic implications of Neoproterozoic, highly fractionated A-type granites from Mianning, South China. *Precambrian Research*, 165(3-4): 190–204.
- Huang, X.L., Xu, Y.G., Lan, J.B., Yang, Q.J., and Luo, Z.Y., 2009. Neoproterozoic adakitic rocks from Mopanshan in the western Yangtze Craton: Partial melts of a thickened lower crust. *Lithos*, 112(3): 367–381.
- Huang, X.L., Niu, Y., Xu, Y.G., Chen, L.L., and Yang, Q.J., 2010. Mineralogical and geochemical constraints on the petrogenesis of post-collisional potassic and ultrapotassic rocks from western Yunnan, SW China. *Journal of Petrology*, 51(8): 1617–1654.
- He Xuexian, Tang Suohan, Zhu Xiangkun and Wang Jinhui, 2007. Precise measurement of Nd isotopic ratios by means of multi-collector magnetic sector inductively coupled plasma mass spectrometry. *Acta Geoscientica Sinica*, 28(4): 405–410 (in Chinese with English abstract).
- Hou Kejun, Li Yanhe, Zou Tianren, Qu Xiaoming, Shi Yurao and Xie Guiqing, 2007. Laser ablation-MC-ICP-MS technique for Hf isotope microanalysis of zircon and its geological applications. *Acta Petrologica Sinica*, 23(10): 2595–2604 (in Chinese with English abstract).
- Hong Tao, You Jun, Wu Chu and Xu Xingwang, 2015. Archean-Paleoproterozoic zircon from a granite porphyry in the Taohua area, western Yunnan and their constrain on the basement of western margin of Yangtze plate. *Acta Petrologica Sinica*, 31 (9): 2583–2596 (in Chinese with English abstract).
- He, W.Y., Mo, X.X., Yu, X.H., He, Z.H., Dong, G.C., Liu, X.B., Su, G.S., and Huang, X.F., 2013. Zircon U-Pb and molybdenite Re-Os dating for the Beiya gold-polymetallic deposit in the western Yunnan Province and geological significance. *Acta Petrologica Sinica*, 29(4): 1301–1310.
- Jiang Yaohui, Jiang Shaoyong, Ling Hongfei and Dai Baozhang, 2006. Petrogenesis of Cu-bearing porphyry associated with continent-continent collisional setting: Evidence from the Yulong porphyry Cu ore-belt, east Tibet. *Acta Petrologica Sinica*, 23(3): 697–706 (in Chinese with English abstract).
- Jiang Xiaojun, Yan Qinggao, Li Wenchang, Li Chao, Wu Peng, Guan Shenjing, Yu Haijun and Li Jinlong, 2018. The metallogenic age and geodynamic setting of the Laojiezi Pb-Ag polymetallic deposit, central Yunnan province: Evidence from Re-Os isotope of sulfides. *Acta Geologica Sinica*, 92(6): 1280–1296 (in Chinese with English abstract).
- Jacobson, S.B., and Wasserburg, G.J., 1980. Sm-Nd isotopic evolution of chondrites. *Earth and Planetary Science Letters*, 50(1): 139–155.
- Lu, Y.J., Robert, K., Peter, A.C., Campbell, M.T., Craig, J.R.H., Li, Z.X., Hou, Z.Q., and Leon, B., 2012. Zircon SHRIMP U-Pb geochronology of potassic felsic intrusions in western Yunnan, SW China: Constraints on the relationship of magmatism to the Jinsha suture. *Gondwana Research*, 22(2): 737–747.
- Lu, Y.J., Robert, K., Anthony, I.S.K., Campbell, M.T., Hou, Z.Q., Craig, J.R.H., Li, Z.X., Peter, A.C., Leon, B., Yang, Z.M., John, C., Elena, A.B., Fred, J., and Noreen J.E., 2013a. Intracontinental Eocene-Oligocene porphyry Cu mineral systems of Yunnan, western Yangtze craton, China: Compositional characteristics, sources, and implication for continental collision metallogeny. *Economic Geology*, 108: 1541–1576.
- Lu, Y.J., Robert, K., Campbell, M.T., Li, Z.X., Craig, J.R.H., Peter, A.C., Hou, Z.Q., Leon, B., John, C., Elena, A.B., and Tang, S.H., 2013b. Geochemical, Sr-Nd-Pb, and Zircon Hf-O isotopic compositions of Eocene-Oligocene shoshonitic and potassic adakite-like felsic intrusions in western Yunnan, SW China: Petrogenesis and tectonic implications. *Journal of Petrology*, 54(7): 1309–1348.
- Lu, Y.J., Campbell, M.T., Li, Z.X., Jourdan, F., Craig, J.R.H., Hou, Z.Q., and Tang, S.H., 2015. Paleogene post-collisional lamprophyres in western Yunnan, western Yangtze Craton: Mantle source and tectonic implications. *Lithos*, 233: 139–161.
- Liang Huaying, Xie Yingwen, Zhang Yuquan and Campbell, I., 2004. The potassic alkaline intrusions constrain the copper mineralization: Case study from Machangqing copper deposit. *Progress in Natural Sciences*, 14(1): 116–120 (in Chinese).
- Liang, H.Y., Campbell, I.H., Allen, C.M., Sun, W.D., Yu, H.X., Xie, Y.W., and Zhang, Y.Q., 2007. The age of potassic alkaline igneous rocks along the Ailao Shan-Red River shear zone: implications for the onset age of left-lateral shearing. *Journal of Geology*, 115(2): 231–242.
- Liang Huaying, Mo Jihai, Sun Weidong, Zhang Yuquan, Zeng Ti, Hu Guangqian and Allen, C.M., 2009. Study on geochemical composition and isotope ages of the Malasongduo porphyry associated with Cu-Mo mineralization. *Acta Petrologica Sinica*, 25(2): 385–392 (in Chinese with English abstract).
- Li Yong, Mo Xuanxue, Yu Xuehui, Huang Xingkai and He Wenyan, 2011. Zircon U-Pb dating of several selected alkali-rich porphyries from the Jinshajiang-Ailaoshan fault zone and geological significance. *Geoscience*, 25(2): 189–200 (in Chinese with English abstract).
- Liu, Y.S., Hu, Z.C., Li, M., and Gao, S., 2013. Applications of LA-ICP-MS in the elemental analyses of geological samples. *Chinese Science Bulletin*, 58(32): 3863–3878.
- Li, X.H., Zhao, H.W., Chung, S.L., Lo, C.H., Wei, G.J., Liu, Y., and Lee, C.Y., 2002. Geochemical and Sr-Nd isotopic characteristics of late Paleogene ultrapotassic magmatism in Southeastern Tibet. *International Geology Review*, 44(6): 559–574.

- Li Wenchang, Yin Guanghou, Liu Xuelong, Lu Yingxiang, Xu Dong, Cao Xiaoming, Zhang Shiquan and Yang Shuran, 2010. ^{40}Ar - ^{39}Ar ages and antimony mineralization of the Pananniuichang porphyry in the Zhongdian area of Yunnan Province. *Geology and Exploration*, 46(2), 267–271 (in Chinese with English abstract).
- Lei, J.S., Zhao, D.P., and Su, Y.J., 2009. Insight into the origin of the Tengchong intraplate volcano and seismotectonics in southwest China from local and teleseismic data. *Journal of Geophysical Research Solid Earth*, 114: B05302.
- Liu, F.T., Liu, J.H., Zhong, D.L., Zhong, J.K., and You, Q.Y., 2000. The subducted slab of Yangtze continental block beneath the Tethyan orogen in western Yunnan. *Chinese Science Bulletin*, 45(5): 466–472.
- Li Guangdou, Nian Hong and Zhang Daohong, 2010. *Metallogenic conditions and prospecting potential of alkali-rich porphyry Cu-Au polymetallic deposits in the western margin of Yangtze plat.* Beijing: Geological Publishing House, 68 (in Chinese with English abstract).
- Middlemost, E.A.K., 1994. Naming materials in the magma/igneous rock system. *Annual Review of Earth & Planetary Sciences*, 37(3–4): 215–224.
- Peccerillo, A., and Taylor, S.R., 1976. Geochemistry of Eocene calc-alkaline volcanic rocks from the Kastamonu area, northern Turkey. *Contributions to Mineralogy and Petrology*, 58(1): 63–81.
- Rui Zongyao, Hou Zengqian, Li Guangming, Zhang Lisheng, Wang Longsheng and Tang Suohan, 2006. Subduction, collision, deep fracture, adakite and porphyry copper deposits. *Geology and Prospecting*, 42(1): 1–6 (in Chinese with English abstract).
- Rapp, R.P., Watson, E.B., and Miller, C.F., 1991. Partial melting of amphibolite/eclogite and the origin of Archean trondhjemites and tonalities. *Precambrian Research*, 51(1–4): 1–25.
- Rapp, R.P., and Watson, E.B., 1995. Dehydration melting of metabasalt at 8–32 kbar: Implications for continental growth and crust-mantle recycling. *Journal of Petrology*, 36(4): 891–931.
- Rushmer, T., 1991. Partial melting of two amphibolites: contrasting experimental results under fluid-absent conditions. *Contributions to Mineralogy and Petrology*, 107(1): 41–59.
- Rushmer, T., 1993. Experimental high-pressure granulites: some applications to natural mafic xenolith suites and Archean granulite terranes. *Geology*, 21(5): 411–414.
- Scherer, C.M., and Mezger, K., 2001. Calibration of the lutetium-hafnium clock. *Science*, 293(5530): 683–687.
- Sen, C., and Dunn, T., 1994. Dehydration melting of a basaltic composition amphibolite at 1.5 and 2.0 GPa: implications for origin of adakites. *Contributions to Mineralogy and Petrology*, 117(4): 394–409.
- Sisson, T.W., Ratajeski, K., Hankins, W.B., and Glazner, A.F., 2005. Voluminous granitic magmas from common basaltic sources. *Contributions to Mineralogy and Petrology*, 148(6): 635–661.
- Sun, S.S., and McDonough, W.F., 1989. Chemical and isotopic systematics of oceanic basalts: implication for mantle composition and processes. In: Saunderson, A.D. and Norry, M.J. (eds), *Magma-tism in the Ocean Basins*. Geological Society, London, Special Publications, 42(1): 313–345.
- Sun, W.H., Zhou, M.F., Gao, J.F., Yang, Y.H., Zhao, X.F., and Zhao, J.H., 2009. Detrital zircon U-Pb geochronological and Lu-Hf isotopic constraints on the Precambrian magmatic and crustal evolution of the western Yangtze Block, SW China. *Precambrian Research*, 172(1): 99–126.
- Sun, C.D., Wu, P., Wang, D., Guan, S.J., and Jiang, X.J., 2017. Geochemistry and zircon U-Pb age of the Yao'an pseudoleucite porphyry, Yunnan Province, China. *Chinese Journal of Geochemistry*, 36(2): 316–328.
- Saunders, A.D., Norry, M.J., and Tarney, J., 1988. Origin of MORB and chemically depleted mantle reservoirs: trace element constraints. *Journal of Petrology*, (Special 1): 415–445.
- Tu Guangchi, 1984. *Geochemistry of stratigraphic deposits of China.* Beijing: Science Press, 73 (in Chinese).
- Tang Suohan, Zhu Xiangkun, Li Jin, Wang Jinhui and Yan Bin, 2010. Separation and isotopic measurement of Sr in rock samples using selective specficresins. *Chinese Journal of Analytical Chemistry*, 38(7): 999–1002 (in Chinese with English abstract).
- Tang Juxing, Wang Qin, Yang Huanhuan, Gao Xin, Zhang Zebin and Zou Bing, 2017. Mineralization, exploration and resource potential of Porphyry-skarn-epithermal copper polymetallic deposits in Tibet. *Acta Geoscientia Sinica*, 38(5): 571–613 (in Chinese with English abstract).
- Taylor, S.R., and McLennan, S.M., 1985. *The continental crust: its composition and evolution.* Oxford: Blackwell of Geophysics, 265.
- Valley, J.W., Lackey, J.S., Cavosie, A.J., Clechenko, C.C., Spicuzza, M.J., Basei, M.A.S., Bindeman, I.N., Ferreira, V.P., Sial, A. N., King, E. M., Peck, W.H., Sinha, A.K., and Wei, C.S., 2005. 4.4 billion years of crustal maturation: oxygen isotope ratios of magmatic zircon. *Contributions to Mineralogy and Petrology*, 150(6): 561–580.
- Wang, J., Yin, A., Harrison, T.M., Marty, G., Zhang, Y.Q., and Xie, G.H., 2001. A tectonic model for Cenozoic igneous activities in the eastern Indo-Asian collision zone. *Earth and Planetary Science Letters*, 188(1): 123–133.
- Wang Jianghai, Yin An, Harrison, T.M., Marty, G., Zhang Yuquan and Xie Guanghong, 2003. Thermo-chronological constraints on two pulses of Cenozoic high-K magmatism in eastern Tibet. *Science in China (Ser. D Earth Science)*, 46(7): 719–729 (in Chinese).
- Wang Denghong, Qu Wenjun, Li Zhiwei, Ying Hanlong and Chen Yuchuan, 2004. The metallogenic concentrated epoch of the porphyry copper (molybdenum) deposits in Jinshajiang-Honghe metallogenic belt: Re-Os isotope dating. *Science in China (Series D)*, 34(4): 345–349 (in Chinese).
- Wiedenbeck, M., Hanchar, J.M., Peck, W.H., Sylvester, P., Valley, J., Whitehouse, M., and Kronz, A., 2010. Further characterization of the 91500 zircon crystal. *Geostandards & Geoanalytical Research*, 28(1): 9–39.
- Winther, K.T., and Newton, R.C., 1991. Experimental melting of hydrous low-K tholeiite: evidence on the origin of Archean cratons. *Bulletin of the Geological Society of Denmark*, 39: 213–228.
- Winther, K.T., 1996. An experimentally based model for the origin of tonalitic and trondhjemitic melts. *Chemical Geology*, 127(1–3): 43–59.
- Wolf, M.B., and Wyllie, P.J., 1994. Dehydration-melting of amphibolite at 10 kbar: the effects of temperature and time. *Contributions to Mineralogy and Petrology*, 115(4): 369–383.

- Wang, X.C., Li, X.H., Li, Z.X., Li, Q.L., Tang, G.T., Gao, Y.Y., Zhang, Q.R., and Liu, Y., 2012. Episodic Precambrian crust growth: evidence from U-Pb ages and Hf-O isotopes of zircon in the Nanhua Basin, central South China. *Precambrian Research*, 222-223: 386–403.
- Weaver, B.L., 1991. The origin of ocean island basalt end-member compositions: trace element and isotopic constraints. *Earth and Planetary Science Letters*, 104(2/4): 381–397.
- Wang Xiaohu, Song Yucai, Zhang Hongrui, Liu Yingchao, Pan Xiaofei and Guo Tao, 2018. Metallogeny of the Baiyangping Lead-Zinc polymetallic ore concentration area, Northern Lanping basin of Yunnan province, China. *Acta Geologica Sinica* (English Edition), 92(4): 1486–1507.
- Xu, L.L., Bi, X.W., Hu, R.Z., Zhang, X.C., Su, W.C., Qu, W.J., Hu, Z.C., and Tang, Y.Y., 2012. Relationships between porphyry Cu-Mo mineralization in the Jinshajiang-Red River metallogenic belt and tectonic activity: Constraints from zircon U-Pb and molybdenite Re-Os geochronology. *Ore Geology Reviews*, 48(1–2): 460–473.
- Xu, L.L., Bi, X.W., Hu, R.Z., Tang, Y.Y., Jiang, G.H., and Qi, Y.Q., 2014. Origin of the ore-forming fluids of the Tongchang porphyry Cu-Mo deposit in the Jinshajiang-Red River alkaline igneous belt, SW China: Constraints from He, Ar and S isotopes. *Journal of Asian Earth Sciences*, 79(2): 884–894.
- Xiong, X.L., Adam, J., and Green, T.H., 2005. Rutile stability and rutile/melt HFSE partitioning during partial melting of hydrous basalt: Implications for TTG genesis. *Chemical Geology*, 218(3): 339–359.
- Xiao, L., and Clemens, J.D., 2007. Origin of potassic (C-type) adakite magmas: Experimental and field constraint. *Lithos*, 95 (3): 399–414.
- Xiao Qianru, Xiong Fuhao, Zhao Han, Feng Xiujun, Wang Qiang and Xiao Yuanfu, 2018. First discovery and zircon U-Pb dating of early Ordovician granitoids in Lincang batholith, western Yunnan: Implications for the presence of Proto-Tethyan orogeny in the Sanjiang region, SW China. *Acta Geologica Sinica* (English Edition), 92(1): 404–405.
- Xu, Y.G., Menzies, M.A., Thirlwall, M.F., and Xie, G.H., 2001. Exotic lithosphere mantle beneath the western Yangtze craton: Petrogenetic links to Tibet using highly magnesian ultrapotassic rocks. *Geology*, 29(9): 863–866.
- Xue Chuandong, Luo Shaoyong, Song Yuchai, Yang Zhiming, Han Yanwei, Huang Qinhui, Li Jin and Wei Aiyang, 2010. Zircon SHRIMP U-Pb dating and its geological significance of Lujiacun quartz-monzonite porphyry in Shangri-la County, northwestern Yunnan Province, China. *Acta Petrologica Sinica*, 26(6): 1845–1855 (in Chinese with English abstract).
- Yan Qinggao, Jiang Xiaojun, Wu Peng, Sun Huiyi and Guan Shenjin, 2017. Zircon SHRIMP U-Pb geochronology and volcanic edifice division of the Laojiezi intraplate alkali-rich volcanic rocks in Yao'an, central Yunnan province. *Acta Geologica Sinica*, 91(8): 1743–1759 (in Chinese with English abstract).
- Yang Xin, Xu Xuhui, Zhang Zhongpei, Liu Yifeng, Zhang Jibian, Liu Xingwang, Xiong Ping and Zhang Jianjing, 2016. Cenozoic magmatism and tectonic framework of western Yunnan, China: Constrained from geochemistry, Sr-Nd-Pb isotopes and fission track dating. *Acta Geologica Sinica* (English Edition), 90(5): 1679–1698.
- Yang Fucheng, Li Wenchang, Liu Xuelong and Wang Shuaishuai, 2017. The late Cretaceous crustal magmatism of the Garzê arc metallogenic belt in Yunnan province, and zircon ages and Hf isotopic evidence of the porphyry Cu-Mo mineralization. *Acta Geologica Sinica* (English Edition), 91 (1): 355–356.
- Zhang Yuquan and Xie Yingwen, 1997. Geochronology and Nd, Sr isotopic characteristics of Alkali-rich intrusive rocks in Ailaoshan- Jinshajiang River. *Science in China* (Series D), 27 (04): 289–293 (in Chinese without English abstract).
- Zhang Yuquan, Xie Yingwen, Li Xianhua, Qiu Huaning, Zhao Zhenhua, Liang Huaying and Zhong Sunlin, 2000. Isotopic characteristic of magmatic rocks in the east of the Tibetan Plateau: rock genesis and its tectonic significance. *Science in China* (Series D), 30(5): 493–498 (in Chinese without English abstract).
- Zeng Pusheng, Hou Zengqian, Gao Yongfeng and Du Andao, 2006. The Himalayan Cu-Mo-Au mineralization in the eastern Indo-Asian collision zone: Constraints from Re-Os dating of Molybdenite. *Geological Review*, 52(1): 72–84 (in Chinese with English abstract).
- Zhou Liqin, Williams, I.S., Liu Jianhui, Ji Zhansheng, Xiao Yuanfu and Liu Dunyi, 2012. Methodology of SHRIMP in-situ O isotopes analysis on conodont. *Acta Geologica Sinica*, 86(4): 611–618 (in Chinese with English abstract).
- Zhang, L.S., and Schärer, U., 1999. Age and origin of magmatism along the Cenozoic Red River shear belt, China. *Contributions to Mineralogy and Petrology*, 134(1): 67–85.
- Zindler, A., and Hart, S.R., 1986. Chemical geodynamics. *Annual Review of Earth and Planetary Sciences*, 14: 493–571.
- Zhao, X.F., Zhou, M.F., Li, J.W., Sun, M., Gao, J.F., Sun, W.H., and Yang, J.H., 2010. Late Paleoproterozoic to early Mesoproterozoic Dongchuan Group in Yunnan, SW China: Implications for tectonic evolution of the Yangtze Block. *Precambrian Research*, 182(1): 57–69.

About the first author

YAN Qinggao, male; born in 1995 in Kaiyuan City, Yunnan Province; Master's degree from Kunming University of Science and Technology, Kunming; working on regional metallogenic dynamics. Email: qinggaoy@126.com; phone: 18788536015.